

## Battery cell electro-thermal modeling and cooling system design

Master of Science Thesis

Qian Sun  
Chengjun Tang



MASTER'S THESIS 2018

# Battery cell electro-thermal modeling and cooling system design

QIAN SUN  
CHENGJUN TANG



Department of Electrical Engineering  
*Division of Electric Power Engineering*  
CHALMERS UNIVERSITY OF TECHNOLOGY  
Gothenburg, Sweden 2018

Battery cell electro-thermal modeling and cooling system design

© QIAN SUN and CHENGJUN TANG, 2018.

Supervisors:

Christèle Grimaud, China Euro Vehicle Technology

Zeyang Geng, Chalmers University of Technology

Examiner: Torbjörn Thiringer, Chalmers University of Technology

Master of Science Thesis Report

Department of Electrical Engineering

Division of Electric Power Engineering

Chalmers University of Technology

SE-412 96 Gothenburg

Telephone +46 31 772 1000

Cover: Schema of the controlled battery cell cooling system

Typeset in L<sup>A</sup>T<sub>E</sub>X

Printed by [ ]

Gothenburg, Sweden 2018



## Abstract

With the rapid development of the electric vehicle industry, the lithium-ion battery plays a more and more important role. By modeling the lithium-ion battery, its behavior can be predicted, and it is easier to manage the battery. The battery model consists of an electrical and a thermal part. The electrical one is an equivalent circuit model, in which the parameters are affected by the temperature and the state of charge (SOC). The heat generated by the electrical model is considered as the input to the thermal model which would result in a new temperature. And the new temperature from thermal model would be fed back to the electrical model. In this way, the electrical model and thermal model can be coupled together. Considering the heat dissipation of the battery cell, a well-designed cooling system is needed. And based on the pre-defined control strategy, the cooling system can regulate the surface temperature of the battery cell in a required operating range, which can prolong the battery life in return.

In this thesis project, a lithium-ion battery was investigated and its electro-thermal model has been built. Different tools, such as the least-square curve fitting and MATLAB Simscape have been used to find the appropriate parameters of electro-thermal model. And the validation results indicated that the model had a relatively high accuracy under high SOC levels.

In parallel to the modeling of the battery, a controlled liquid cooling system has been designed. By using the output signal from an Arduino micro-controller, a peristaltic pump, driven by a 12V DC motor was controlled, and thus the coolant flow was controlled. Bang-bang control strategy was used in this thesis, and the results indicated that the designed cooling system managed to control the battery temperature. However, due to the limitation of the coolant pump, the battery temperature showed a slowly increasing trend even though the pump was engaged at its maximum capacity. A more powerful pump can help to solve this problem, and Simscape simulation showed that when trebling the coolant pump capacity, the battery temperature can be regulated in the demand range.

Keywords: Lithium-ion battery, electro-thermal model, battery modeling, cooling system design.



# Acknowledgements

This thesis work has been carried out at the Division of Electric Power Engineering, Department of Electrical Engineering at Chalmers University of Technology, Gothenburg, Sweden and China Euro Vehicle Technology, Gothenburg, Sweden.

We would like to express our thanks to the following people,

- Our supervisor Zeyang Geng and examiner Prof. Torbjörn Thiringer at Chalmers University of Technology.
- Our supervisor Dr. Christèle Grimaud at China Euro Vehicle Technology.

Qian and Chengjun, Gothenburg, August 2018



# Contents

<b>1</b>	<b>Introduction</b>	<b>1</b>
1.1	Background . . . . .	1
1.2	Problem overview . . . . .	1
1.3	Aim . . . . .	2
1.4	Scope . . . . .	2
1.4.1	Battery electro-thermal modelling . . . . .	2
1.4.2	Cooling system design . . . . .	2
1.5	Sustainable issues . . . . .	2
<b>2</b>	<b>Theory</b>	<b>3</b>
2.1	Battery in vehicles . . . . .	3
2.2	Lithium-ion battery . . . . .	3
2.2.1	Description of battery cell . . . . .	3
2.3	Battery model concepts . . . . .	4
2.3.1	The equivalent circuit model . . . . .	4
2.3.1.1	0 RC circuit model . . . . .	4
2.3.1.2	1 RC circuit model . . . . .	5
2.3.1.3	2 RC circuit model . . . . .	5
2.3.2	Thermal model . . . . .	6
2.3.2.1	Lumped parameter model . . . . .	6
2.3.2.2	Cauer model . . . . .	7
2.4	Electrical and thermal model coupling . . . . .	7
2.5	Control theory . . . . .	8
2.5.1	Bang-bang control . . . . .	9
2.5.2	PID control . . . . .	9
<b>3</b>	<b>Experimental setup</b>	<b>11</b>
3.1	General setup . . . . .	11
3.2	Equipment . . . . .	12
3.2.1	Data acquisition . . . . .	12
3.2.2	Charging/discharging the battery . . . . .	12
3.2.3	Cooling system . . . . .	12
3.2.4	Parameter identification . . . . .	12
3.2.5	Temperature measurement . . . . .	12
3.2.6	Flowrate measurement . . . . .	12
3.3	Calibration . . . . .	13

3.3.1	Calibration setup . . . . .	13
3.3.2	Calibration of the peristaltic pump . . . . .	14
3.3.2.1	Procedures . . . . .	14
3.3.2.2	Results . . . . .	15
3.3.3	Calibration of the flow meter . . . . .	15
3.3.3.1	Procedures . . . . .	15
3.3.3.2	Results . . . . .	16
<b>4</b>	<b>Electrical modeling</b>	<b>17</b>
4.1	RC parameters identification . . . . .	17
4.1.1	Test sequence . . . . .	17
4.1.2	Parameter identification method . . . . .	18
4.1.3	Parameter identification results . . . . .	19
4.2	Electrical model validation . . . . .	22
4.2.1	Validation model . . . . .	22
4.2.2	Validation results . . . . .	23
<b>5</b>	<b>Thermal modelling</b>	<b>25</b>
5.1	Battery temperature response . . . . .	25
5.1.1	Styrofoam box thermal parameters measurement . . . . .	25
5.1.2	1C discharging battery temperature measurement . . . . .	27
5.1.3	Electrical and thermal model coupling . . . . .	28
5.2	Measurement of specific heat capacity . . . . .	30
<b>6</b>	<b>Cooling system</b>	<b>33</b>
6.1	Cooling plate design . . . . .	33
6.2	Physical setup . . . . .	35
6.3	Control of the cooling system . . . . .	35
6.4	Performance of cooling system . . . . .	36
6.5	Simulation of cooling system in MATLAB . . . . .	37
6.5.1	Thermal model establishment . . . . .	37
6.5.2	Simulink models . . . . .	38
6.5.3	Comparison between the practical cooling system and the simulation . . . . .	39
6.5.4	Model modification . . . . .	40
6.5.4.1	Thermal model modification . . . . .	41
6.5.4.2	Power losses modification . . . . .	43
6.5.5	Comparison between the practical cooling system and the simulation after modification . . . . .	43
6.5.6	Simulation with more powerful pump scenarios . . . . .	44
<b>7</b>	<b>Discussion</b>	<b>47</b>
7.1	Conclusion . . . . .	47
	<b>Bibliography</b>	<b>49</b>
<b>A</b>	<b>Appendix 1</b>	<b>I</b>

A.1	Bang-bang control Arduino code . . . . .	I
A.2	PID control Arduino code . . . . .	II

## Abbreviations

<b>BTMS</b>	Battery Thermal Management System
<b>CFD</b>	Computational Fluid Dynamics
<b>EV</b>	Electric Vehicle
<b>HEV</b>	Hybrid Electric Vehicle
<b>ICE</b>	Internal Combustion Engine
<b>LFP</b>	Lithium Iron Phosphate
<b>LMO</b>	Lithium Manganese Oxide
<b>LTO</b>	Lithium Titanate
<b>NMC</b>	Lithium Nickel Cobalt Manganese Oxide
<b>OCV</b>	Open Circuit Voltage
<b>SOC</b>	State of Charge



# 1

## Introduction

### 1.1 Background

With the stringent requirement on the emission from automobiles [1], electric vehicles (EV) and hybrid electric vehicles (HEV) have been experiencing a rapid development. Among the numerous components which comprise electric vehicles and hybrid vehicles, the battery is one of the most important parts. Due to the advantages such as high energy density, various types of lithium-ion batteries are extensively used as the traction source in EVs and HEVs [2].

However, even though the lithium-ion batteries have dominated the consumer electronics market, the technology used for the EV and HEV is far from full maturity and the further development needs to be fulfilled [3]. The lithium-ion battery related research is extremely essential to optimize the vehicles' cost, performance, etc. Different methods from the electrical, thermal, mechanical and electrochemistry perspectives have been used to establish different battery models, and the dynamic behaviors of the battery regarding different charging/discharging rates and temperatures have been investigated. Among the various battery models, electro-thermal modeling is commonly used to study the relationship between the current and the temperature of battery.

In parallel with the battery modeling, a cooling system should also be designed to control the battery temperature, thus enhancing the performance of the battery, prolonging the battery life time, and ensuring the battery safety. Normally in commercial electric vehicles, the battery thermal management system (BTMS) with various cooling technologies is used to fulfill the above tasks [4]. Different control strategies can be employed to optimize the thermal management of the battery, such as the bang-bang, PID and feedforward control.

### 1.2 Problem overview

With the fast development of the lithium-based battery technology, a large number of battery models have been built, whereas different models emphasize particularly on different battery properties [5]. Similarly, some different battery cooling systems have been developed, while an effective cooling system, such as with a suitable cooling power and control strategy, is rarer.

### 1.3 Aim

One of the aims of this thesis is to establish a suitable battery cell electro-thermal model structure, which can well represent the dynamic behavior of a targeted battery. Another aim is to implement an effective cooling system for the battery cell, considering the coolant's temperature, the velocity of the flow, etc.

### 1.4 Scope

#### 1.4.1 Battery electro-thermal modelling

In this project, all the experiments are conducted with a commercial lithium-ion battery. The electrical model for this battery is an empirical model which consists of one internal resistance with several RC branches. Based on the heat generation equation, a thermal model, which can be coupled with the electrical model is also developed.

#### 1.4.2 Cooling system design

The battery cooling system is designed by minimizing the temperature swing of the battery. The cooling strength can be controlled by controlling the flow rate. A temperature controller is implemented in the cooling system, ensuring that the battery surface temperature remains within the required margin.

### 1.5 Sustainable issues

An appropriate battery electro-thermal model contributes to precisely studying of battery problems, which can help to enhance the performance of electric vehicles. Thus more people would like to purchase and drive electric vehicles, and there will be less emissions, resulting in a enhanced sustainable development. Furthermore, a cooling system manages to protect the battery from overheating and the battery is thus expected to have a longer life time. Less materials for manufacturing the battery will then be used, which is also good for the environment.

# 2

## Theory

### 2.1 Battery in vehicles

With the increasing number of cars, the fuel consumption and exhaust gas pollution are becoming more and more serious. In the foreseeable condition of technology, the trend of developing more EVs is inevitable [6]. The battery has become one of the most important components and its advanced level determines the cost and performance of the EVs [7].

All the traction batteries used in automotive industry are rechargeable (secondary batteries), and they have two major categories. One is ambient-temperature operating batteries with either aqueous or non-aqueous electrolytes. Another one is high-temperature batteries with molten or solid electrolytes [3]. The lithium based battery is one kind of commonly used battery technology, and usually consists of lithium-ion and lithium-metal polymer types. In this thesis project, lithium-ion battery is the main study object.

Compared to fossil fuels (12,000 Wh/kg [8], gasoline fuel), the energy density of today's batteries (100 - 150 Wh/kg [8], lithium-ion battery) is significantly lower, which is one of the bottlenecks in the development of EVs [8]. To reach a reasonable driving range, large battery packs have to be installed and the cost and the weight are thus expected to increase, although the price per kilogram goes down.

### 2.2 Lithium-ion battery

#### 2.2.1 Description of battery cell

Figure 2.1 shows the tested lithium-ion battery in this thesis, a commercial 26 Ah li-ion pouch cell. Based on the data sheet offered by the supplier, its voltage range (continuous) is from 2.8 V to 4.15 V, corresponding to 0 to 100 % SOC level.

The negative electrode is made up of the natural graphite and the negative tap material is the nickel plated copper. The positive electrode is a mixture of the lithium manganese oxide (LMO) and the lithium nickel cobalt manganese oxide (NMC). And the material for the positive tap is aluminum [9].

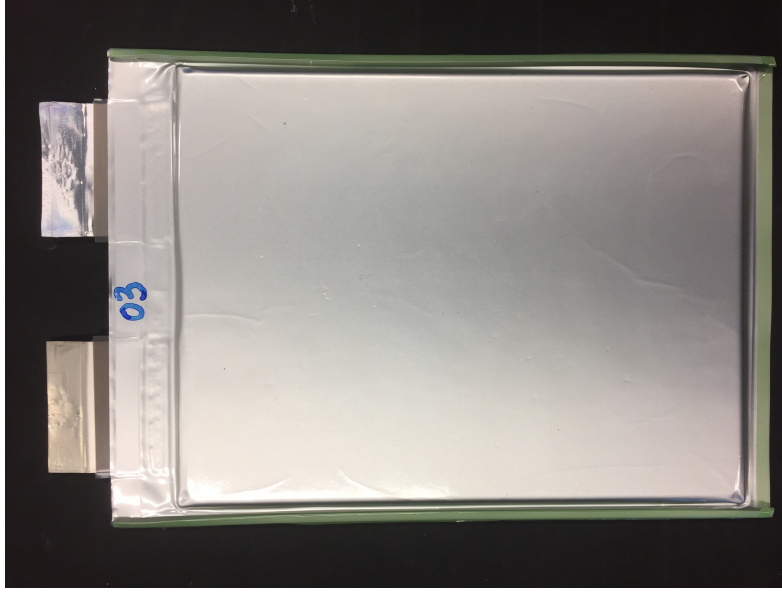


**Figure 2.1:** The Lithium-ion battery cell used in this thesis

## 2.3 Battery model concepts

It is quite important to design an economical battery management system in vehicles, and using an accurate battery model is vital to dimension the cooling system. The following models have been introduced in different literatures.

- **The electrochemical model**

The electrochemical model is based on the electrochemistry equations, which can bring an accurate model of small cells and can be used to predict the cell performance [5]. However, the exact behavior of the battery cell is far from being fully modelled yet.

- **The equivalent circuit model (ECM)**

The ECM contains various models, and the battery behaviors can be represented by using equivalent electrical circuits with different electrical elements [10]. In this thesis project, an ECM is used to model the battery cell.

### 2.3.1 The equivalent circuit model

#### 2.3.1.1 0 RC circuit model

Figure 2.2 shows the 0 RC circuit model, which comprises of the ideal voltage source  $U$ , the cell internal resistance  $R$  and the terminal voltage  $V$ . This model is good for the fast computation since there is only one parameter to be determined, which is the internal resistance  $R$ . However, this model cannot properly capture the dynamic response of the battery.

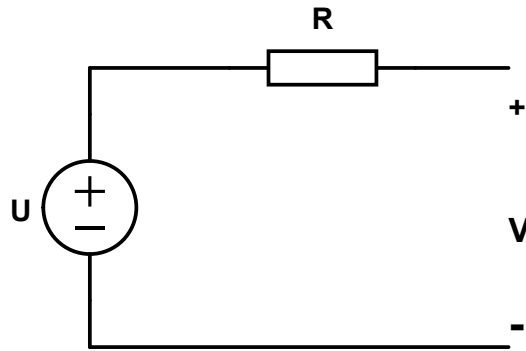


Figure 2.2: 0 RC circuit model

### 2.3.1.2 1 RC circuit model

Figure 2.3 shows the 1 RC circuit model, which consists of the ideal voltage source  $U$ , the cell internal resistance  $R_0$ , the terminal voltage  $V$  and one RC branch ( $R_1$  and  $C_1$ ). The additional RC branch contributes to the time constant, which makes this model to have a better dynamic behaviour compared to the 0 RC model.

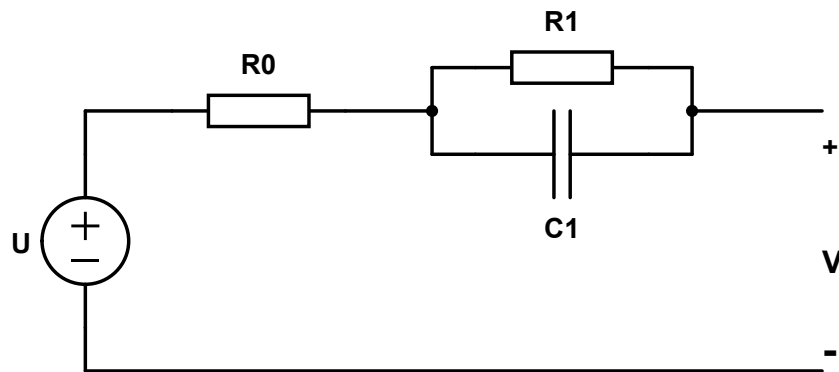
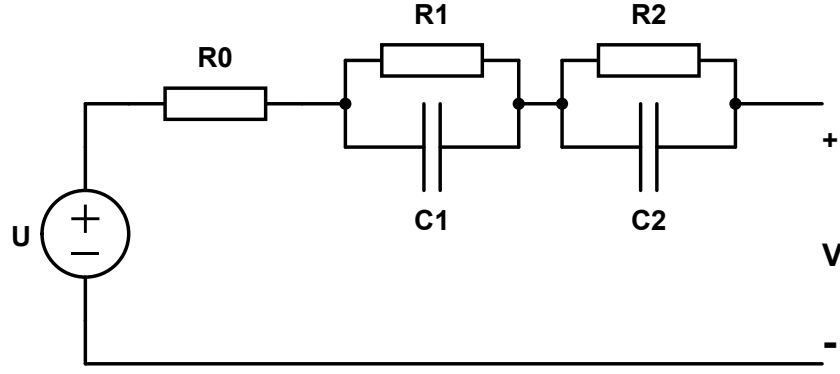


Figure 2.3: 1 RC circuit model

### 2.3.1.3 2 RC circuit model

Figure 2.4 shows the 2 RC circuit model, which includes the ideal voltage source  $U$ , the cell internal resistance  $R_0$ , the terminal voltage  $V$  and two RC branches ( $R_1 + C_1$  and  $R_2 + C_2$ ). Two RC branches means two different time constants, therefore this model can represent a more delicate dynamic behavior of the battery compared with the 1 RC circuit model.



**Figure 2.4:** 2 RC circuit model

## 2.3.2 Thermal model

### 2.3.2.1 Lumped parameter model

Due to the fact that the heat transfer transient is existing in the physical set-up, the lumped parameter model is used to describe the thermal model [11]. A typical lumped parameter thermal model is shown in Figure 2.5, where  $P$  is the heating power generated in the battery,  $C$  is the thermal capacity of the battery and the set-up,  $R$  is the thermal resistance of the insulation,  $T_c$  is the temperature of the battery and  $T_a$  is the ambient temperature.

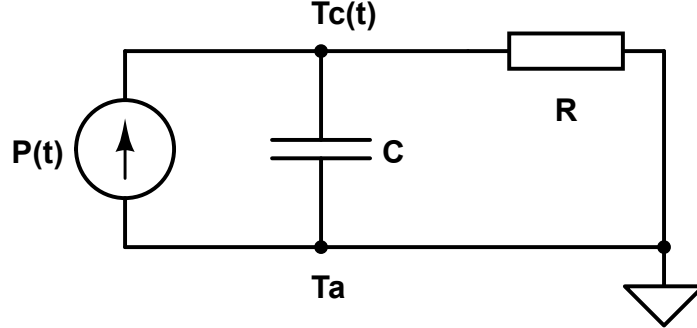


**Figure 2.5:** A typical lumped parameters thermal model

The transient temperature response  $T_c(t)$  meets the following equation [12],

$$C \frac{dT_c(t)}{dt} = P + \frac{T_a - T_c(t)}{R} \quad (2.1)$$

For a step input  $P$ , the solution to (2.1) is,

$$T_c(t) = PR(1 - e^{-\frac{t}{RC}}) + T_a \quad (2.2)$$

It can be seen that the battery temperature  $T_c(t)$  meets an exponential equation, and Figure 2.6 shows the typical curve of  $T_c(t)$  when the battery dissipates a constant power  $P$ . The battery temperature  $T_c(t)$  starts with the ambient temperature  $T_a$ , and reaches a steady state temperature after a sufficiently long time period. Based

on (2.2), it means that the difference between the steady state temperature and initial ambient temperature is decided by the thermal resistance of the insulation  $R$ , whereas the transient battery temperature is initially fully decided by the thermal capacity  $C$  and  $R$ .

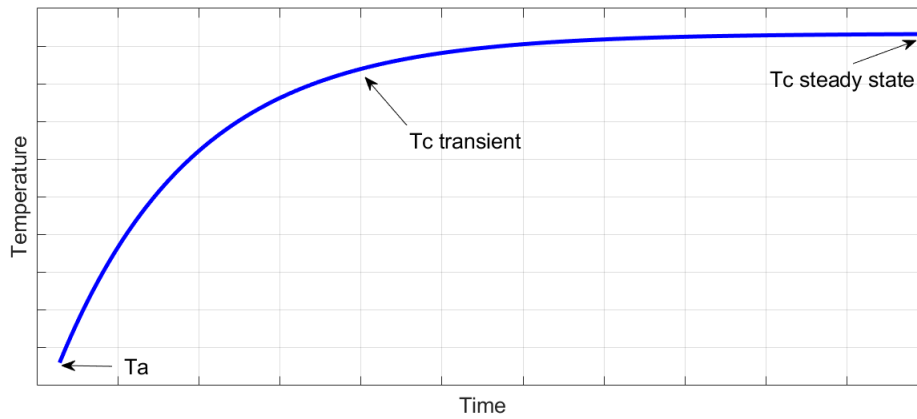


**Figure 2.6:** Temperature transient for a step input power

### 2.3.2.2 Cauer model

For the transient temperature response, another thermal model can be used which is called the Cauer model. The Cauer model consists of several RC branches, and different RC branches represent different physical parts of the thermal system. Taking an IGBT power module for example, the Cauer model can be used to describe the different physical layers in the module. Figure 2.7 shows a Cauer model with several branches.

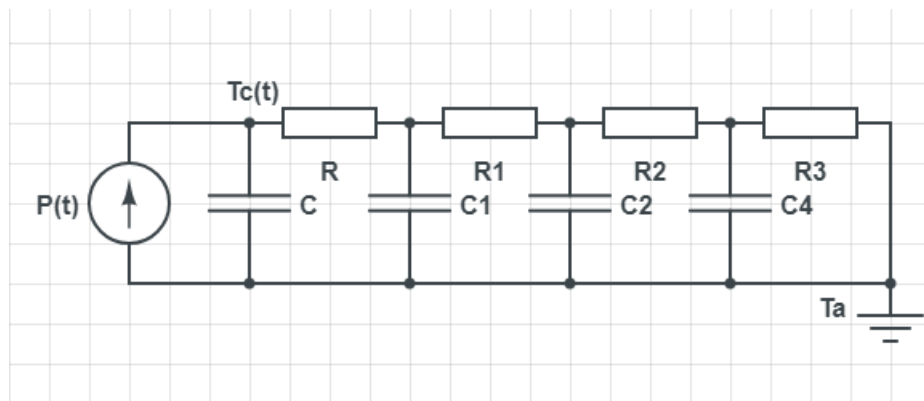


**Figure 2.7:** The Cauer model

## 2.4 Electrical and thermal model coupling

Figure 2.8 shows the battery electro-thermal model, which couples the electrical and thermal model closely. The initial inputs of the electrical model are the discharge

current, the SOC level and the temperature. The inputs to the electrical model result in a heat signal to the thermal model, which will cause a temperature output signal from the thermal model. And then the new temperature is fed back to the electrical model, since the new temperature affects the the electrical parameters such as the internal resistance, capacitance, etc.

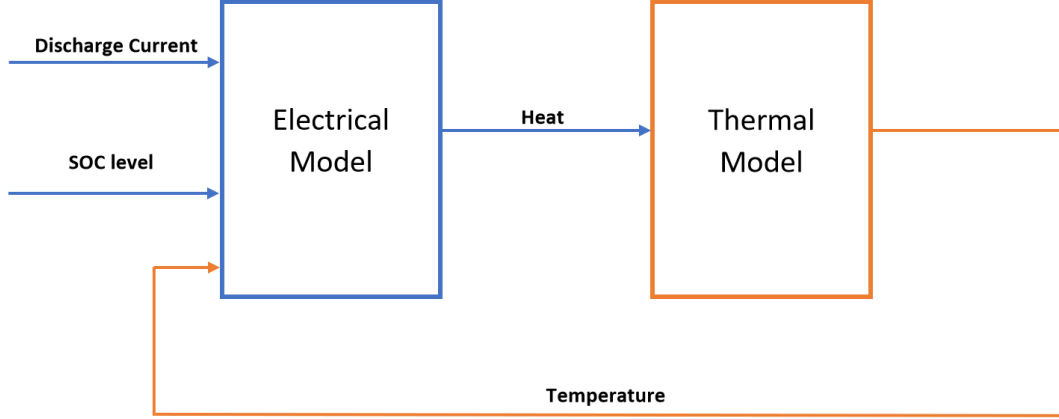


**Figure 2.8:** Coupling between the electrical and thermal model

The heat generated by the battery cell during the charge and discharge process is expressed by the following equation,

$$Q = Q_J + Q_E = I^2 R + IT \frac{\partial U}{\partial T} \quad (2.3)$$

where  $Q_J$  is the joule heat,  $Q_E$  is the entropy heat,  $I$  is the current through the battery cell,  $R$  is the total resistance of the battery cell,  $T$  is the temperature of the battery cell and  $\frac{\partial U}{\partial T}$  is the entropy coefficient.

The joule heat plays a main role in the battery heat generation when the discharging current is larger than 1C rate current, Moreover, the entropy heat is a bit complicated, therefore only the joule heat is considered in this thesis project. This means that when the battery is discharged with a constant 1C rate current, a good knowledge of the internal resistance  $R$  is needed. This can give a relatively accurate battery heat generation model in return.

## 2.5 Control theory

Control theory is an interdisciplinary branch of engineering and mathematics that deals with the behavior of dynamic system with inputs, and how their behavior is modified by the feedback [13]. The common control algorithms include logic control, bang-bang control, linear control and so on.



### 2.5.1 Bang-bang control

A bang-bang controller, also known as the hysteresis controller, has lower and upper bounds and it is controlled by switching between two states, such as ON and OFF. Also it has an advantage of solving control problems in different areas, such as robotics, rocket flight and so on [14].

### 2.5.2 PID control

A proportional-integral-derivative controller (PID controller) is a control loop feedback mechanism. The PID controller is by far the most common control algorithm and most practical feedback loops are based on PID control [15]. Figure 2.9 shows a typical PID control block diagram. Inside the feedback loop,  $r(t)$  is the set/desired value,  $e(t)$  is the error signal that would be sent to the PID controller,  $u(t)$  is the controller output that would be sent to the plant model and  $y(t)$  is the output of the plant model that would be compared again with  $r(t)$ . The aim of the PID controller is to enable the model output  $y(t)$  to follow the set/desired value  $r(t)$ .

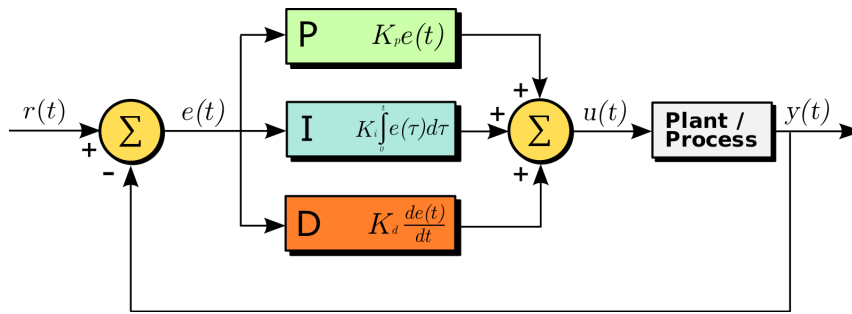


**Figure 2.9:** A typical PID controller



# 3

## Experimental setup

### 3.1 General setup

Figure 3.1 shows setup of the whole system. On the left corner of this figure is the GAMRY device, which can be used to charge and discharge the battery under certain currents. When the battery cell is discharged with 1C rate current, a certain amount of heat can be generated, and the battery temperature increases.

Then a peristaltic pump is used to draw water from the water reservoir (with the air cooling) to cool the battery cell temperature down. And the pump is controlled by an Arduino control board, which can also collect the measured battery surface temperature data in real time. One of the benefits to use an Arduino board is that different control algorithms can be easily implemented, due to the abundant open source online libraries. In the meantime, the Arduino board also reads the temperature of the inlet and outlet coolant, and obtains the flow rate from the flow meter. With the temperature difference between the inlet and outlet as well as the flow rate, the heat being taken away can be calculated.

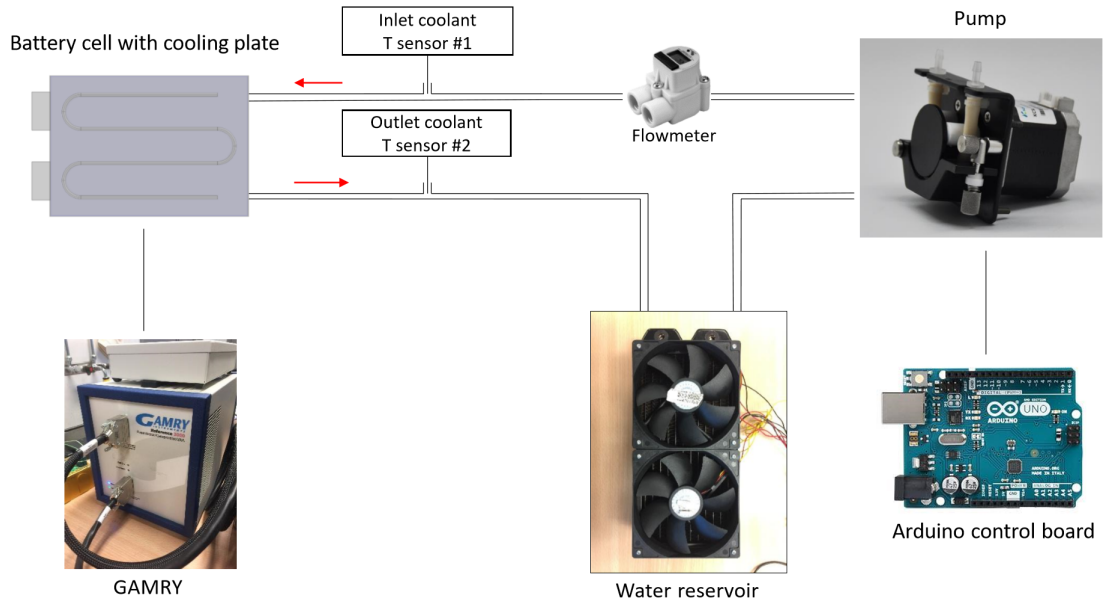


Figure 3.1: General setup of the whole system

## 3.2 Equipment

Many experiment and measurement equipment were used for different purposes in this project. In addition to the following equipment, hoses, connectors and cooling plates were also used.

### 3.2.1 Data acquisition

IPETRONIK temperature and voltage module: this is a 24-channel analog measurement module (16 for the temperature and 8 for the voltage), which is compatible with the K type thermocouple.

### 3.2.2 Charging/discharging the battery

GAMRY Reference 3000 & 30k booster: this set of equipment is useful for charging/discharging the battery. The maximum charging/discharging current it can provide is 30 A.

### 3.2.3 Cooling system

12V Peristaltic Pump: the pump is driven by a 12V DC motor and can produce a flow range from 19 - 200 ml/min according to the manufacturer's data.

Arduino UNO Microcontroller: the UNO (SMD EDITION) is the most used board and is designed based on the ATmega328P microprocessor. It has 14 digital input/output pins, 6 analog inputs and a 16 MHz quartz crystal.

### 3.2.4 Parameter identification

Climatic Chamber KK115: the chamber can produce a temperature range from -10 to +60 °C; the relative humidity ranges from 30 - 90 %.

### 3.2.5 Temperature measurement

K type thermocouple, PTFE, exposed welded tip (for battery): the measured temperature range is from -75 to +250 °C and it is ideal for test and development applications.

DS18B20 temperature sensor (for fluid and battery): a digital thermometer, which has  $\pm 0.5$  % and can measure temperature from - 10 to +85 °C.

### 3.2.6 Flowrate measurement

DIGMESA FHK flowmeter: the flowmeter is a general-purpose device, which measures the flow rate from 0.027 - 0.58 L/min and its measurement accuracy is  $\pm 2$  %.

## 3.3 Calibration

### 3.3.1 Calibration setup

The calibration setup of the pump and the flowmeter includes the power supply, the fan, the pump, the flow-meter and an Arduino microcontroller. Figure 3.2 shows the connection of the power supply, the pump and the fan (for cooling the pump). There are three channels from the power supply: the first one (left) is for the pump, the second one (middle) is for the flowmeter and the third one (right) is for the fan.

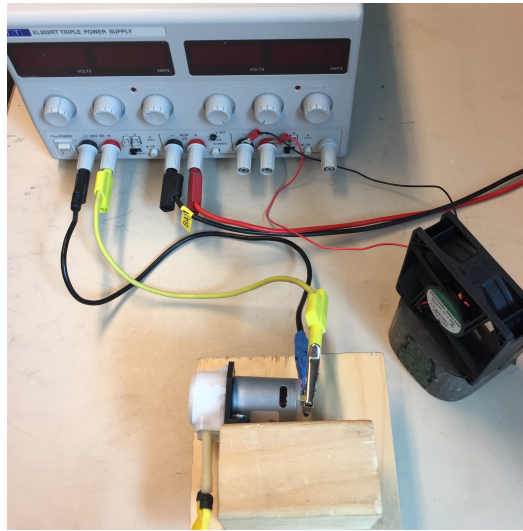


**Figure 3.2:** Power supply and the pump

Figure 3.3 shows the connection of the pump and the flowmeter. With the power supply, the pump draws water from one container and transports it to the other container through the flowmeter, which generates the output signal to the Arduino at the same time.

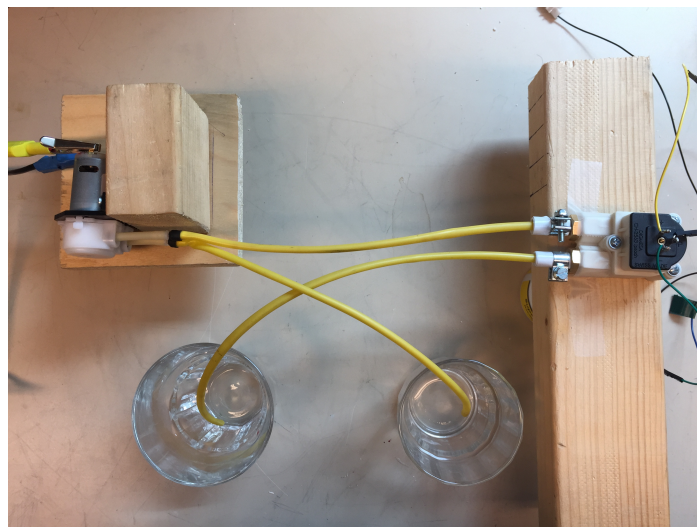


**Figure 3.3:** Pump and the flowmeter

### 3. Experimental setup

---

Figure 3.4 shows the connection of the flowmeter and the Arduino UNO (SMD edition) board. And there are three pins on the flowmeter: positive, ground and signal. They are connected with a designed circuit, shown in Figure 3.6. Its output is the TTL signal, which stands for the transistor-transistor logic. Then the output is fed into the digital input of the Arduino board, which counts the pulse numbers and display the results on the computer screen.

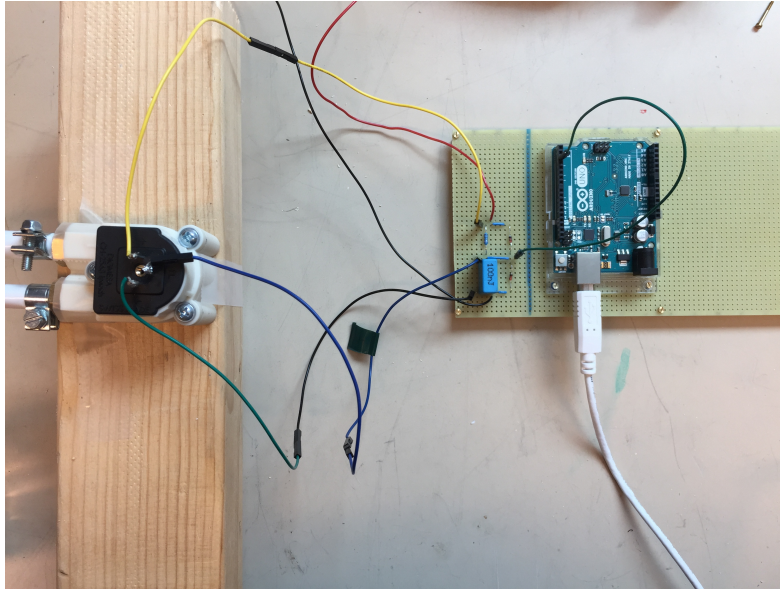


**Figure 3.4:** Flowmeter and the Arduino

#### 3.3.2 Calibration of the peristaltic pump

In order to determine the accuracy and the traceability of the measurements, a calibration was done for the peristaltic pump.

##### 3.3.2.1 Procedures

The peristaltic pump was calibrated via the following steps:

1. Connect the peristaltic pump with the power supply;
2. Run the pump, measure the water mass in the container, convert the mass to the volume and record the time;
3. Repeat the step 2 for 5 times;
4. Calculate the flow rate in average;
5. Adjust the voltage level from 9 - 12 V, with an increment of 0.25 V and start over from the step 2;
6. Record the final data and plot the calibration results using MATLAB.

### 3.3.2.2 Results

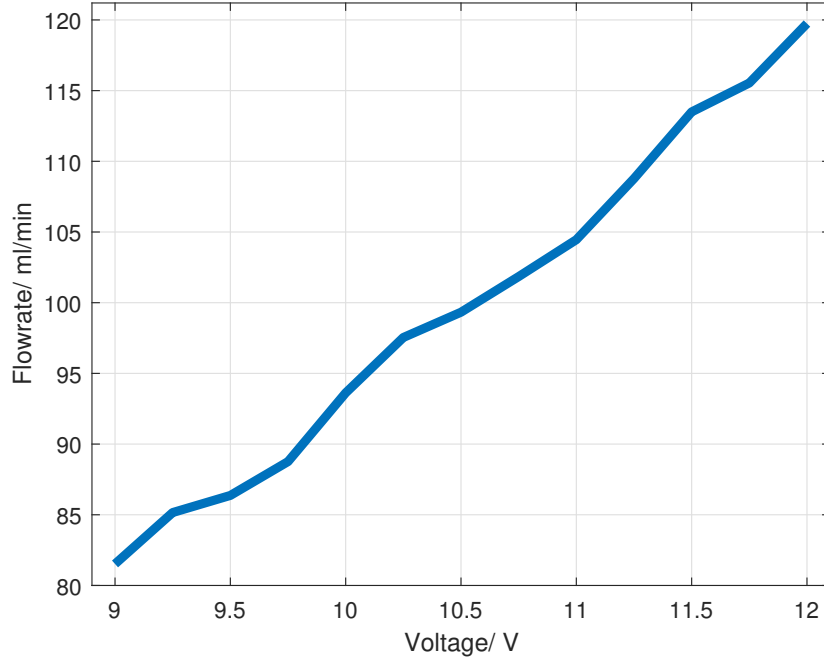


**Figure 3.5:** Characteristics curve of the peristaltic pump

From Figure 3.5, it can be observed that the pump's flow-rate increases with the voltage and the pump is working relatively linearly from 9 - 12 V.

### 3.3.3 Calibration of the flow meter

In order to determine the accuracy and the traceability of the measurements, the calibration was done for the flow meter.

#### 3.3.3.1 Procedures

The flowmeter was calibrated via the following steps:

1. Connect the flowmeter in a designed circuit shown in Figure 3.6;
2. Supply the running water with the pump to the flow meter and read the pulse number via Arduino;
3. Wait 1 min to stabilize the water flow and measure the mass of the water that stored in the container;
4. Record the time and convert the the mass of the water to the volume;
5. Repeat the step 2 - 4 for 5 times;
6. Calculate the pulse number and flow rate in average;
7. Adjust the voltage level from 9 - 12 V, with an increment of 0.25 V and start over from the step 2.

### 3. Experimental setup

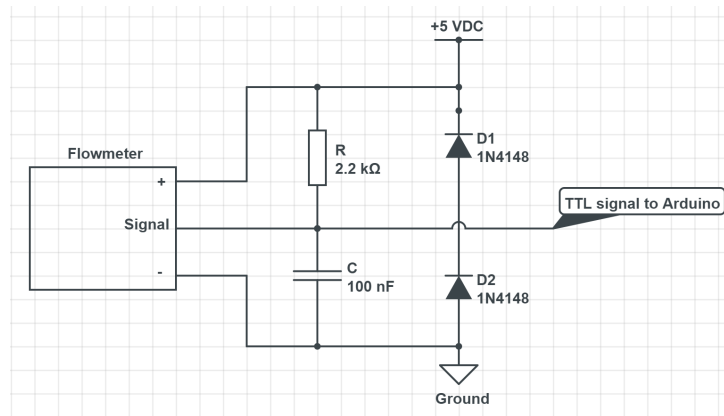


**Figure 3.6:** The designed circuit schematic for the flowmeter

#### 3.3.3.2 Results

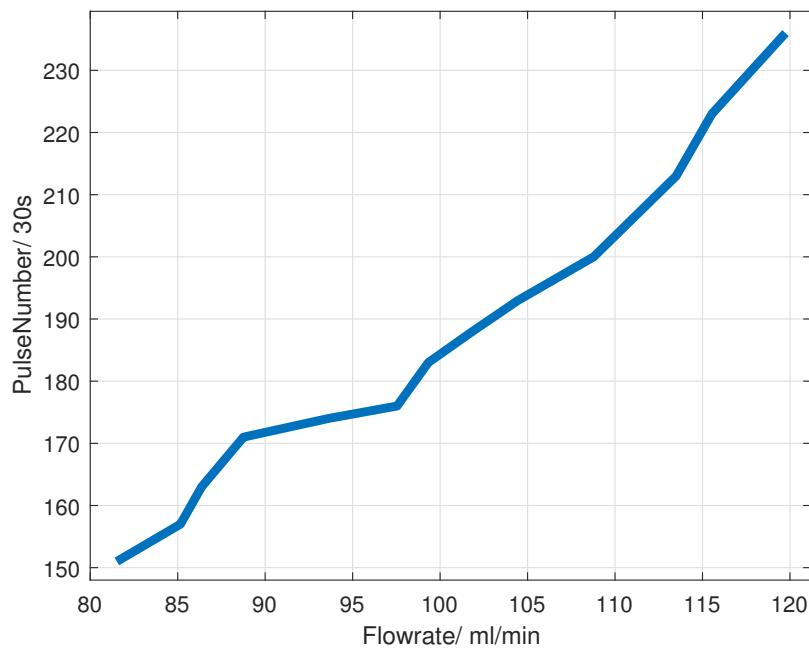


**Figure 3.7:** Characteristics curve of the FHK flowmeter

From Figure 3.7, it can be seen that the flowmeter's measured flow-rate versus the pulse number increases with the flow-rate and the flow meter is working relatively linearly from the range 80 - 120 ml/min.



# 4

## Electrical modeling

### 4.1 RC parameters identification

#### 4.1.1 Test sequence

Since the RC parameters as shown in Figure 2.4 are sensitive to SOC level and temperature of the battery cell, the RC parameters of the equivalent circuit needs to be determined by conducting pulse tests under different SOC levels and temperatures.

The capacity of the battery cell is 26 Ah, and a 1C rate is chosen to be the discharge current, which is 26 A. By using the climate chamber, the 10 °C, 20 °C and 30 °C conditions are established. Totally 20 discharge pulses are used and each pulse lasts for 180 seconds, which means that the battery SOC will decrease 5% after each pulse. After the 180s pulse discharge, the battery cell is relaxed for 2 hours. Figure 4.1 shows the battery cell terminal voltage response when the pulse test is conducted under 10 °C and 100 % SOC.

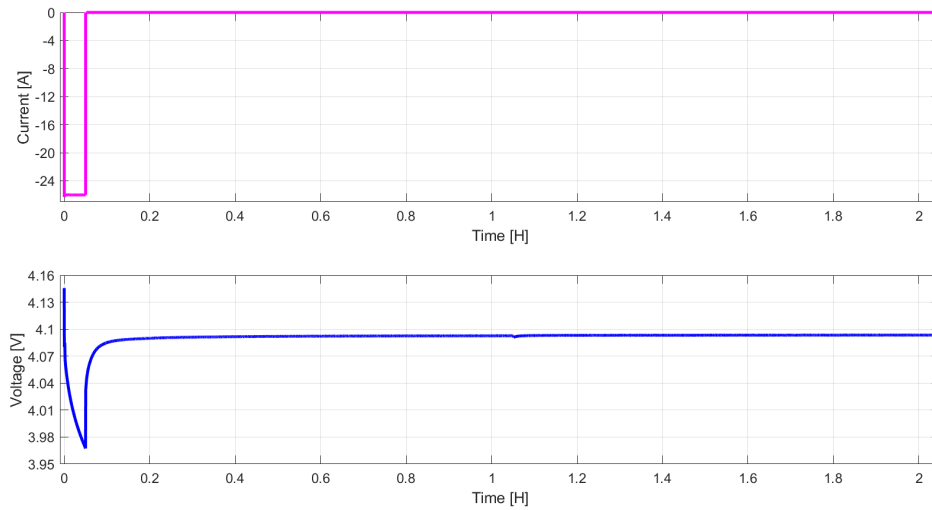


**Figure 4.1:** One current pulse test and battery voltage response curve

By applying the least square fitting method on the battery relaxation period, the RC parameters can be identified. Figure 4.2 shows the estimated voltage response based on the RC model with the corresponding relaxation curve.

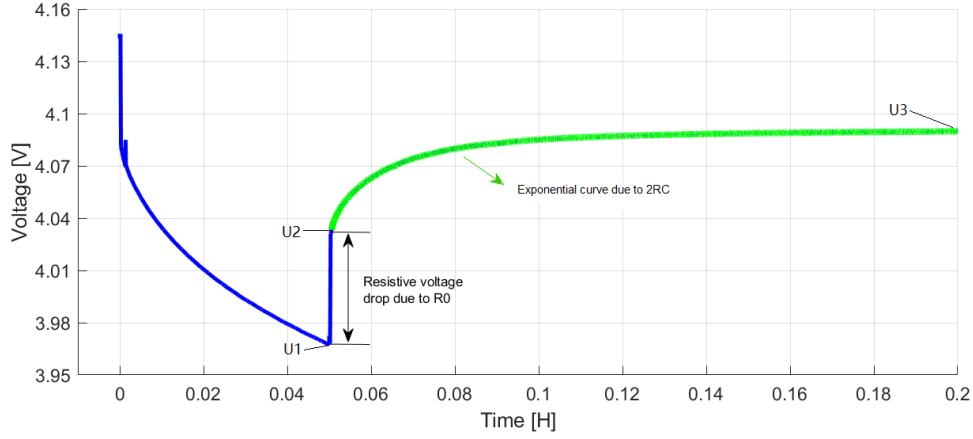


**Figure 4.2:** Relationships of RC with relaxation curve

### 4.1.2 Parameter identification method

Based on the relaxation curve 4.2,  $R_0$  can be identified by using the following equation,

$$R_0 = \frac{U_2 - U_1}{I} \quad (4.1)$$

where  $U_1$  is the voltage when the discharge pulse is ended,  $U_2$  is the instant voltage increase after the discharge pulse,  $I$  is the discharge pulse current.

The other RC parameters can be identified by using the non-linear least square curve fitting method on the green part in Figure 4.2 [16]. The relaxation voltage  $U$  is assumed to have the following behavior,

$$U = U_3 - a_1 e^{(-b_1 t)} - a_2 e^{(-b_2 t)} \quad (4.2)$$

where  $U_3$  is the steady state voltage of relaxation curve,  $a_1$ ,  $b_1$ ,  $a_2$ ,  $b_2$  are the coefficients need to be fitted.

And the relationships between the coefficients and RC parameters are listed as following:

$$\tau_1 = \frac{1}{b_1} \quad (4.3)$$

$$R_1 = \frac{a_1}{I(1 - e^{-b_1 t_{pulse}})} \quad (4.4)$$

$$C_1 = \frac{I(1 - e^{-b_1 t_{pulse}})}{a_1 b_1} \quad (4.5)$$

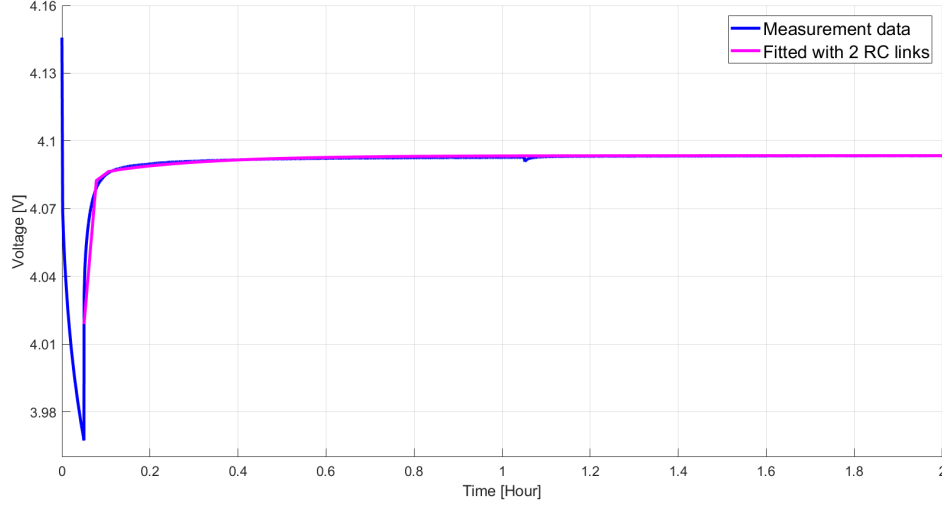
$$\tau_2 = \frac{1}{b_2} \quad (4.6)$$

$$R_2 = \frac{a_2}{I(1 - e^{-b_2 t_{pulse}})} \quad (4.7)$$

$$C_2 = \frac{I(1 - e^{-b_2 t_{pulse}})}{a_2 b_2} \quad (4.8)$$

where  $\tau_1$  and  $\tau_2$  are the time constants of corresponding RC networks,  $t_{pulse}$  is the duration of current discharge pulse, which is 180 s in this case.

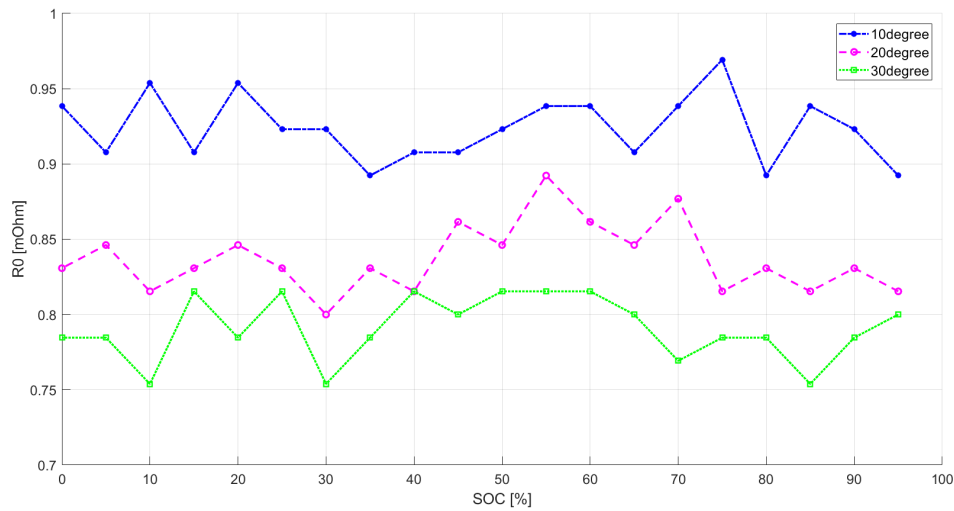
Figure 4.3 gives one example of the fitted voltage curve with the measurement data. It can be seen that this model set-up can fit the measurement data quite well.



**Figure 4.3:** Measured data and fitted data

### 4.1.3 Parameter identification results

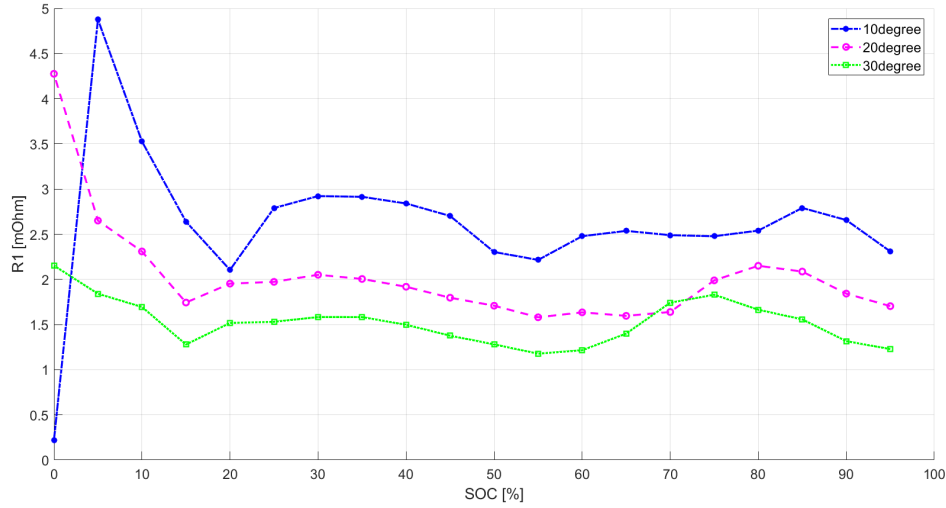
The identified RC parameters with the corresponding temperature and SOC level are shown in Figure 4.4 to 4.10 respectively.



**Figure 4.4:**  $R_0$  with temperature and SOC variation

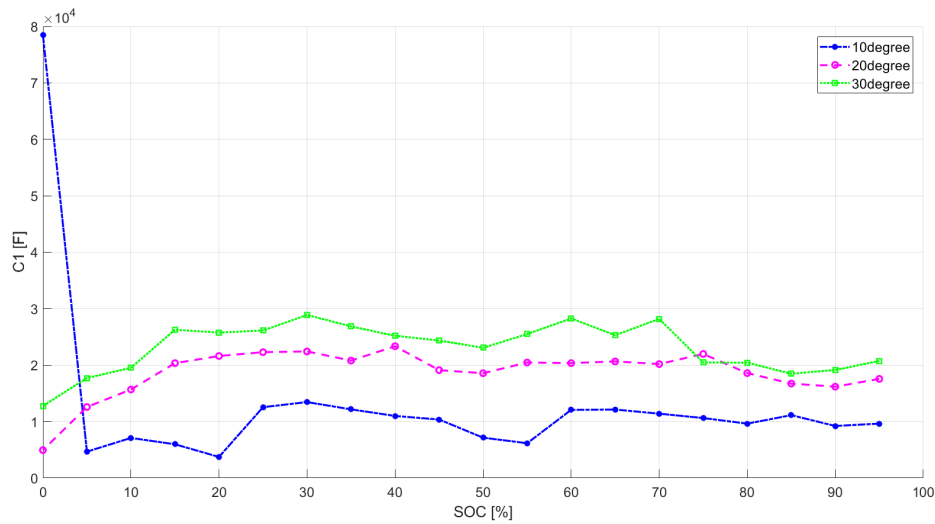
The above Figure 4.4 shows the  $R_0$  results which acquired by using (4.1). It can be

seen that when the ambient temperature increases from 10 °C to 30 °C, the internal resistance  $R_0$  decreases. At the same time,  $R_0$  fluctuates with the SOC level.



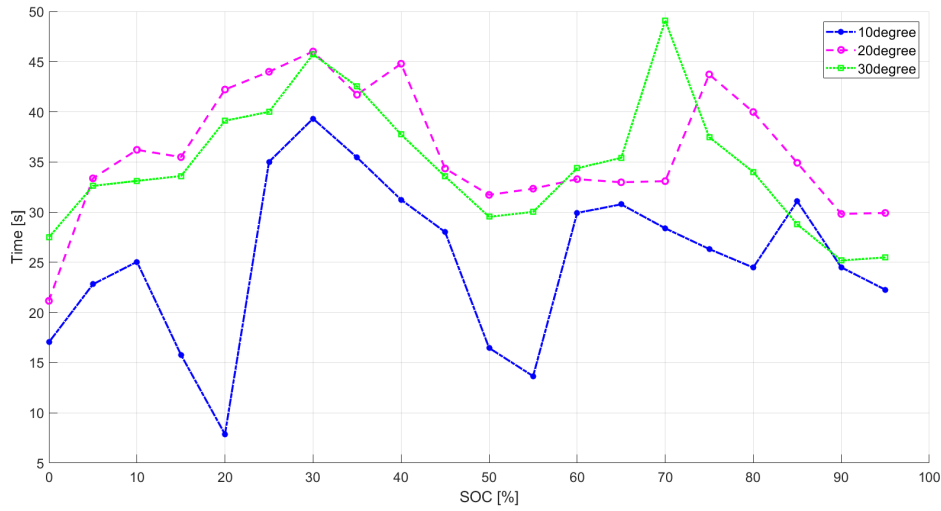
**Figure 4.5:**  $R_1$  with temperature and SOC variation

The results of the ECM parameter  $R_1$  is shown in Figure 4.5. The effect of the ambient temperature shows the same trend on internal resistance  $R_1$ . However, one significant difference compared with Figure 4.4 is that  $R_1$  increases a lot when the SOC level is lower than 15 %. This means that  $R_1$  is not only affected by the temperature but also by the battery SOC level.



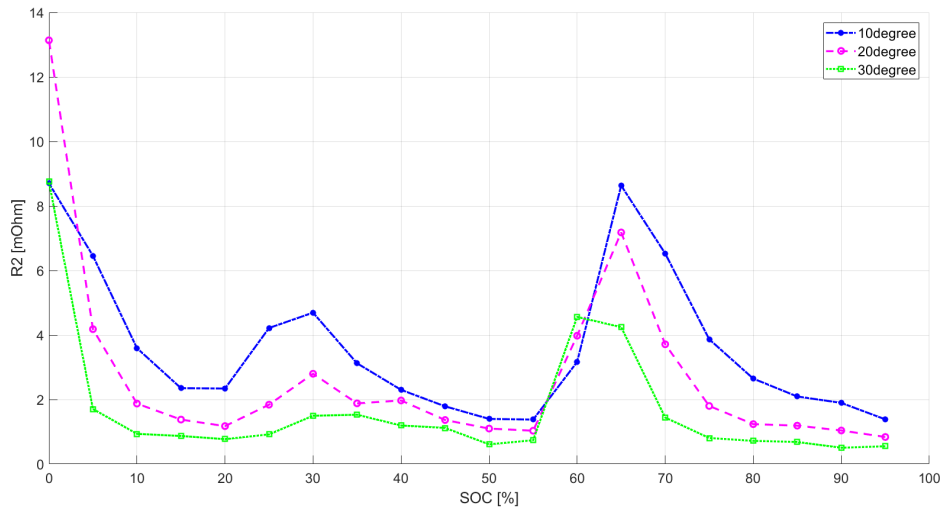
**Figure 4.6:**  $C_1$  with temperature and SOC variation

Figure 4.6 shows the results of ECM parameter  $C_1$ . When the ambient temperature is increased, the  $C_1$  value is increased as well, and this shows an opposite trend to the internal resistance.



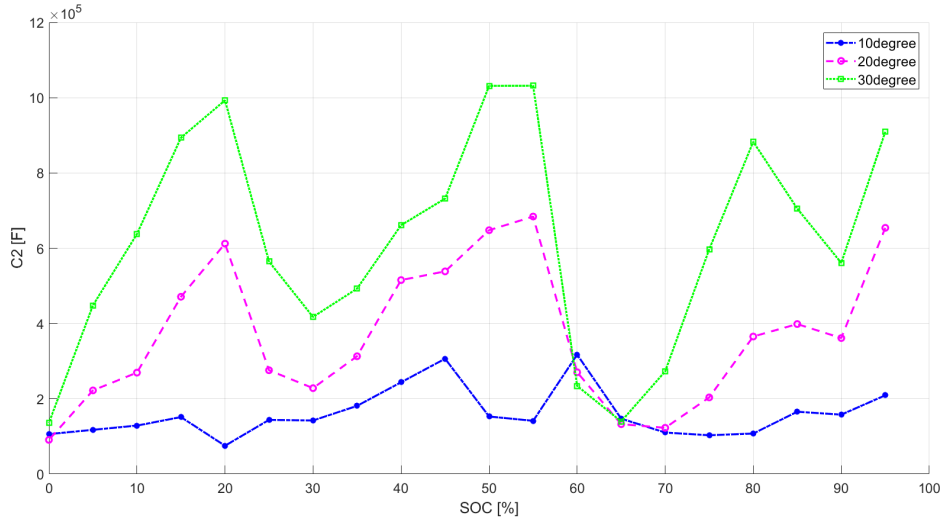
**Figure 4.7:**  $\tau_1$  with temperature and SOC variation

Figure 4.7 shows the time constant  $\tau_1$  of the first RC link in the ECM. However,  $\tau_1$  fluctuates quite a lot with the temperature and SOC level, none of a clear trend can be found in this figure.



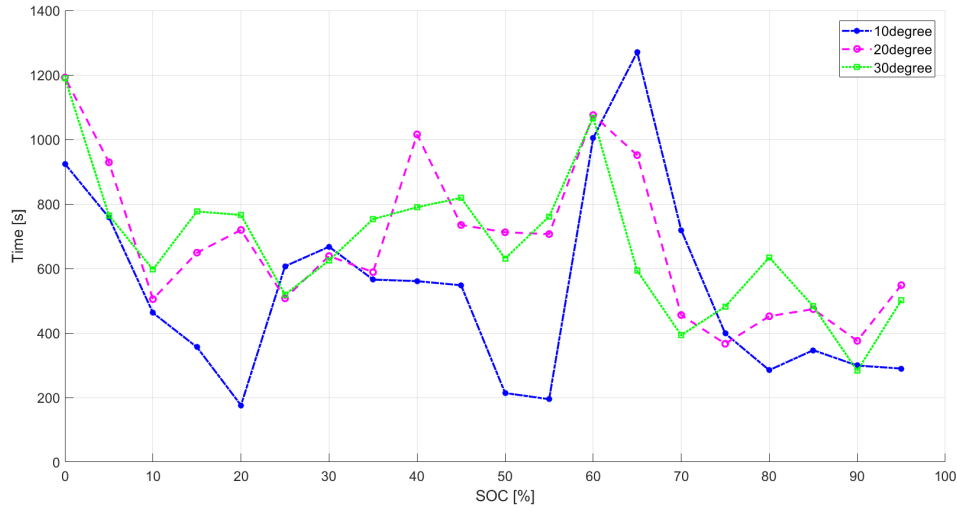
**Figure 4.8:**  $R_2$  with temperature and SOC variation

Figure 4.8 gives the  $R_2$  results, which shows that  $R_2$  almost has the same pattern as the internal resistance  $R_1$ , except that the  $R_2$  values bump around 65 % SOC level. The reason for this is maybe that the relaxation period around the 65 % SOC level is not long enough, which may lead to an inaccurate curve fitting.



**Figure 4.9:**  $C_2$  with temperature and SOC variation

Figure 4.9 and 4.10 show the results when using the second RC link in the ECM. And the patterns of these parameters are similar to  $C_1$  and  $\tau_1$ .



**Figure 4.10:**  $\tau_2$  with temperature and SOC variation

From the above results it can be inferred that the battery internal resistance is closely related to the ambient temperature and the battery SOC level.

## 4.2 Electrical model validation

### 4.2.1 Validation model

Since the ECM only consists of electrical elements, MATLAB Simscape can be used to simulate the battery electrical model [17]. Figure 4.11 shows the 2RC equivalent

circuit model which is built in MATLAB Simscape. Due to the fact that the electrical parameters change with the SOC level, a series of look-up tables are used for different parameters in the model.

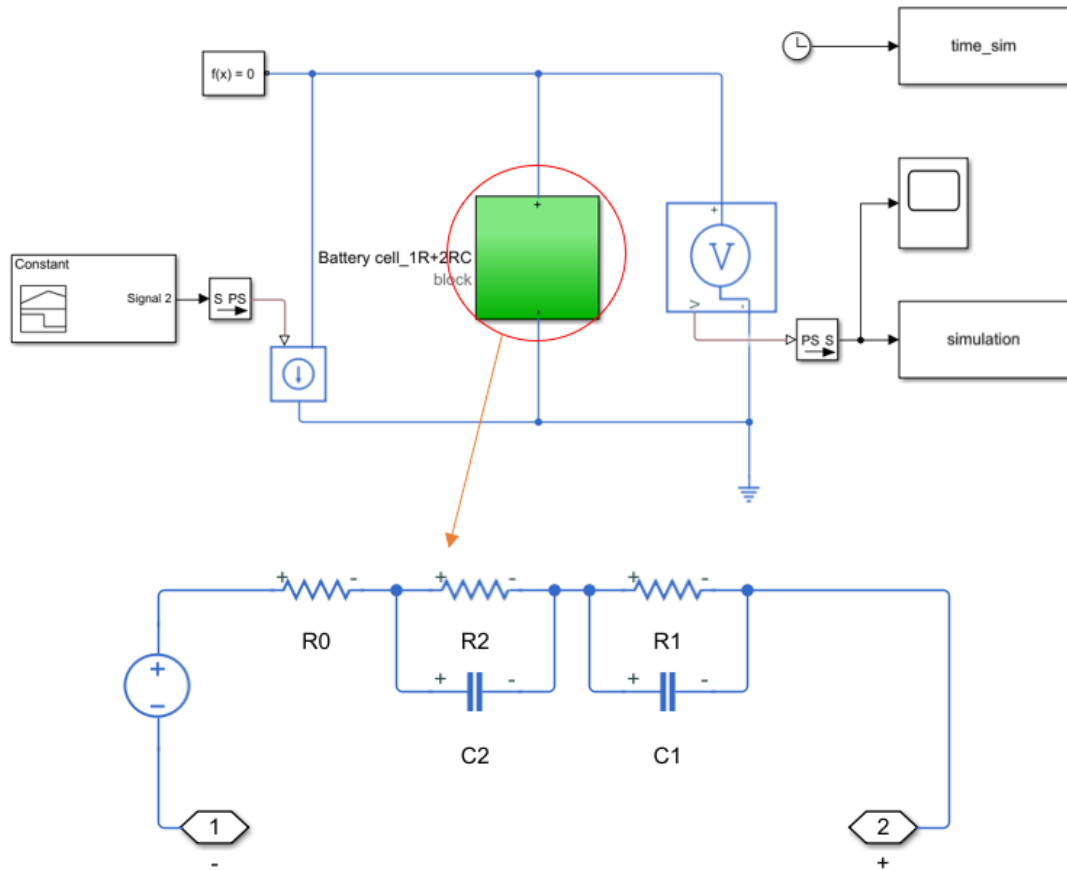


**Figure 4.11:** Battery validation model used in MATLAB Simscape

### 4.2.2 Validation results

Since the room temperature is around 30 °C when conducting the experiment, the battery electrical parameters which were identified under 30 °C condition are used for the input of the Simscape model to do the validation. The simulation result is shown in Figure 4.12, in which the experiment data is also plotted.

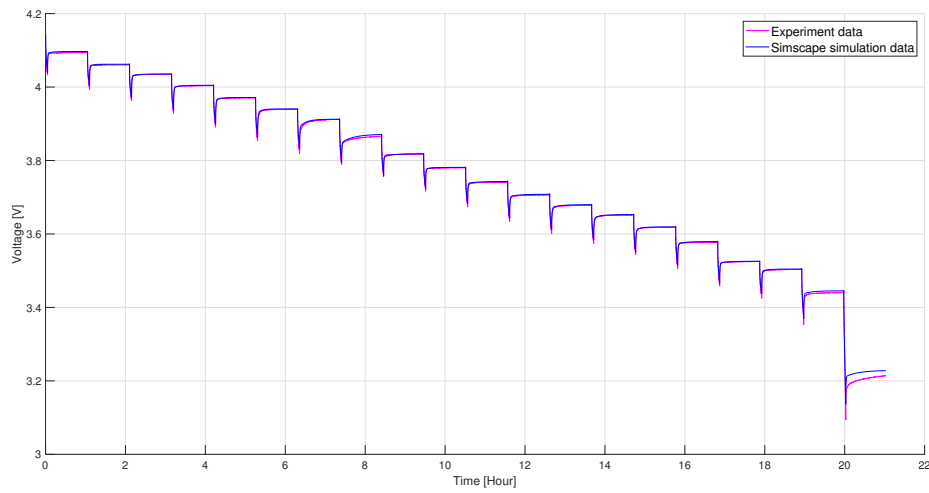


**Figure 4.12:** Comparison between experiment and Simscape simulation result

It can be seen that the measured battery terminal voltage matches quite well with the simulation result when the battery SOC level is high. However, at low SOC level, the difference between the experimental and simulation results becomes significant. This means that the electrical parameters under low SOC level are not accurate, which is caused by the insufficient relaxation time and inaccurate curving fitting results.



# 5

## Thermal modelling

### 5.1 Battery temperature response

When the battery is discharged and charged, due to the existence of internal resistance in the battery cell, a certain amount of heat is generated in the battery cell and can increase the temperature of battery. And free air convection, most of the heat of the battery will dissipate into the air thus not much temperature increase could be observed. One styrofoam box is made to emulate the real application case and capture the temperature response of battery cell. The used styrofoam box in this thesis project is shown in Figure 5.1.

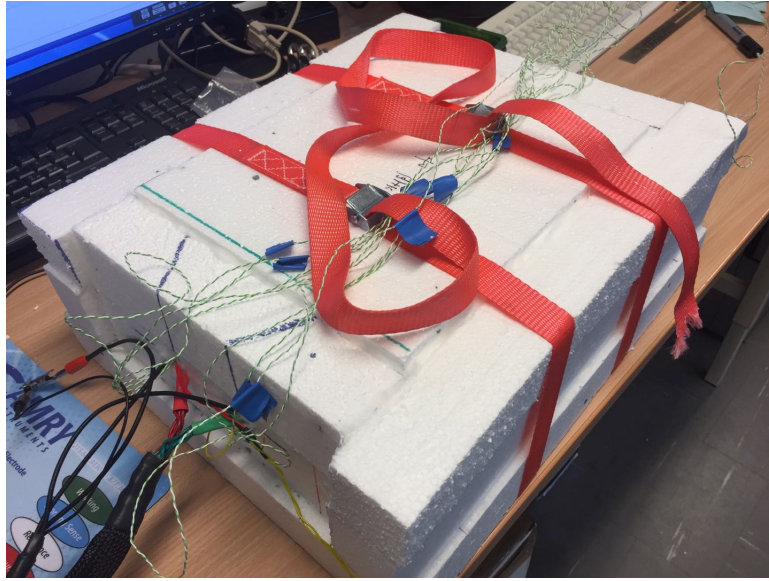


**Figure 5.1:** The built styrofoam box

#### 5.1.1 Styrofoam box thermal parameters measurement

The first step of the thermal modelling is to measure the thermal resistance and capacity of the physical set-up. By using the heater to heat the battery cell with a known power input and the thermocouple to measure the temperature, the thermal parameters can be identified. The assembly of the battery cell, the heater and the thermocouples are shown in Figure 5.2.

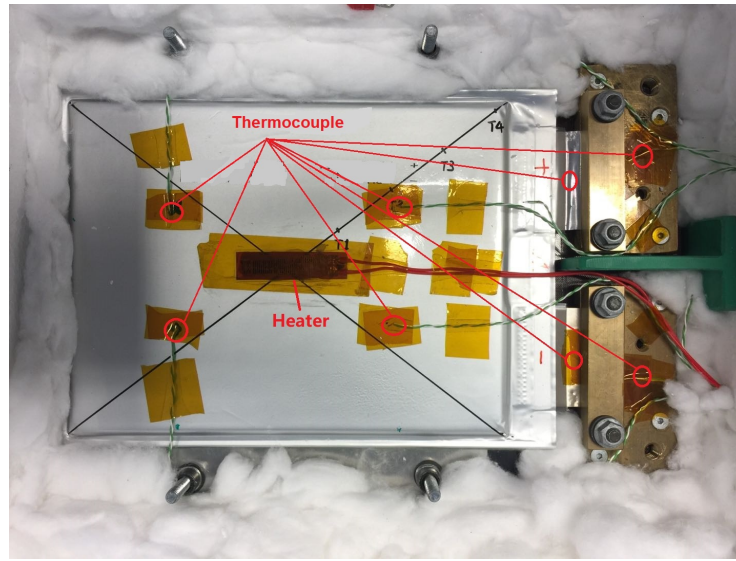


**Figure 5.2:** Assembly of the battery cell, the heater and the thermocouples

From the above figure, it can be seen that the heater is located in the middle of battery cell. Four thermocouples are used to measure the body temperature of the cell and two thermocouples are used to measure the temperature on the tab. The other two thermocouples are used to measure the temperature of the brass holder.

The heater is connected with a power supply which provides 2.53 W (14.04 V and 0.18 A). Figure 5.3 shows the average temperature response of the battery cell. During heating, two stages can be observed: the temperature increases with an exponential trend in the beginning, and it remains stable after about 18 hours. When shutting down the power supply of the heater, the temperature starts to drop. It can be noted that the ambient temperature varied a lot since the temperature during the day is different from the temperature in the evening, which is hard to be avoided.

Based on the description in the theory part, the temperature response of the battery cell meets (2.2) during the heating process. Thus, by using the non-linear least square curve fitting method in MATLAB, the thermal resistance  $R$  and thermal capacity  $C$  of the styrofoam assembly can be identified. Figure 5.4 shows the fitted temperature and actual temperature in the battery cell.

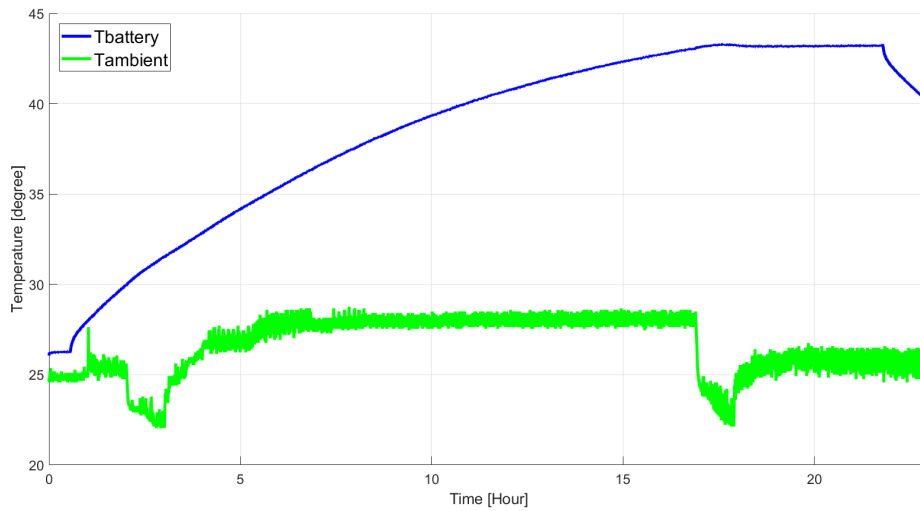


**Figure 5.3:** Battery temperature response when using the heater

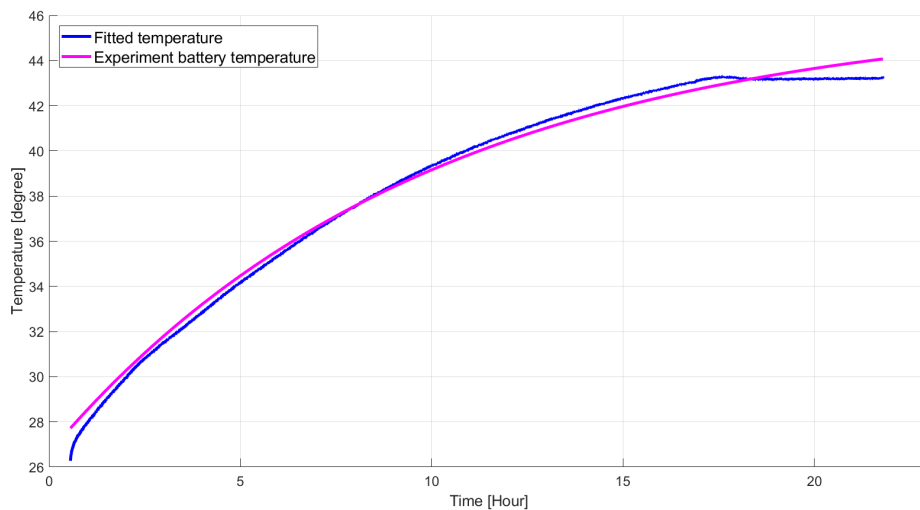


**Figure 5.4:** Fitted temperature and actual temperature in the battery cell

Table 5.1 shows the thermal resistance and capacitance of the styrofoam box assembly.

**Table 5.1:** Styrofoam box thermal parameters

Thermal parameters	Thermal resistance (R)	Thermal capacity (C)
Value	7.6 K/W	4635.8 J/K

### 5.1.2 1C discharging battery temperature measurement

After the thermal parameters of the assembly is measured, the battery cell is discharged with 1C rate current and the temperature of battery cell is measured. One

of the reasons to use the 1C rate discharging current is that this thesis wants to investigate the battery heat generation in vehicles, which means that discharging the battery can more intuitively illustrate the usage of the battery to propel the vehicles. Another reason is the maximum current of the GAMRY and booster can reach is 30 A, thus, 26 A is within the range and is easier to control the discharge time.

Figure 5.5 shows the temperature response of battery cell body and tabs under 1C rate current discharge. It can be seen that the body of the battery cell increases about 2.5 °C while the positive tab temperature increases more than 4 °C. The reason to this is that the positive tab of the battery cell is made of aluminum, and the oxidation layer on the aluminum surface increases the contact resistance of the positive tab, which generates significant heat when the battery is discharged with large current. By polishing the aluminum and adding some electrical conductive paste on the positive tab before each experiment, this issue can be remedied.

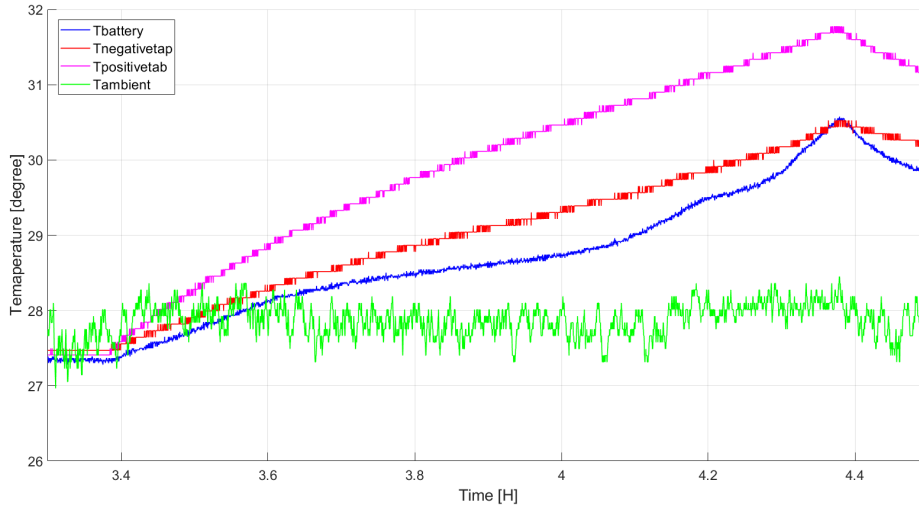


**Figure 5.5:** Battery cell temperature under 1C current discharge

### 5.1.3 Electrical and thermal model coupling

As discussed in the theory part, the electrical and thermal model can be coupled closely. Figure 5.6 shows the process of how to do the electrical and thermal model coupling.

The simulated battery temperature response and the experiment data are compared in Figure 5.7. It can be seen that the simulation result is close to the experiment result when the battery starts to discharge, which means the battery is at high SOC level. However, when it is at a low SOC level, the difference between the two data becomes apparently, which is brought by the inaccurate electrical model at low SOC level. On the other hand, the battery cell was considered as a homogenous object when performing the simulation, whereas the actual battery cell has different

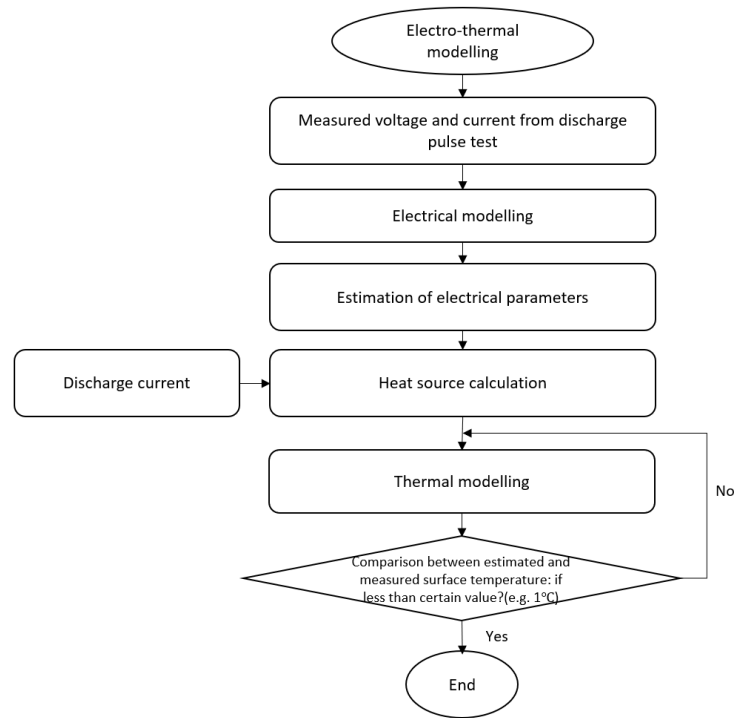


**Figure 5.6:** Electro-thermal modelling flow chart

thermal conductivities on different directions, which means different placement of thermocouples on the battery will also bring different comparison results.

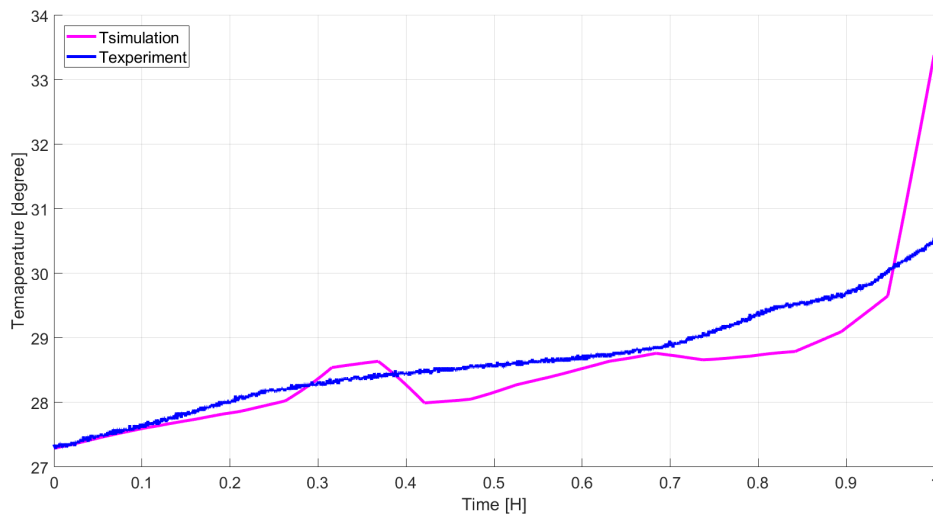


**Figure 5.7:** Comparison of simulated and experiment temperature

Figure 5.8 gives the voltage comparison results of the simulation and experiment, from which we can find the same deviation when at the low SOC level.

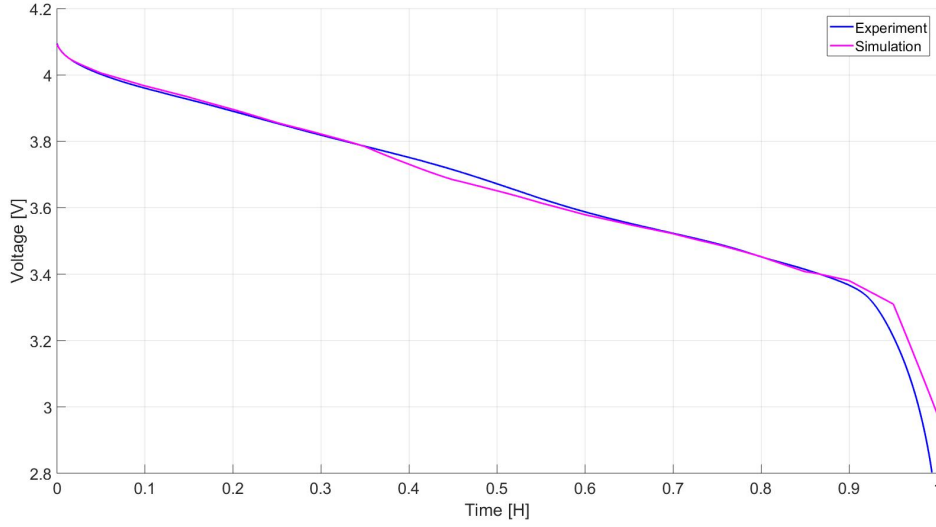


**Figure 5.8:** Comparison of simulated and experiment voltage

## 5.2 Measurement of specific heat capacity

Maleki et al. have proposed two methods to measure the specific heat of a lithium-ion battery in [18]. In this thesis project, the first method which uses the cooling transient is introduced and applied.

Firstly, a dummy cell with a known material which has almost the same size as the actual battery cell is heated up to a certain temperature. Then the dummy cell is put inside a Styrofoam box, designed with thermal insulation material such as cotton filled to prevent internal convection cooling. The heat loss from the assembly is determined by the external heat transfer coefficient  $h$ , which can be acquired by solving the following equation,

$$\dot{Q} = hA(T - T_a) + mC_p \frac{dT}{dt} \quad (5.1)$$

where  $\dot{Q}$  is the heat supplied by the heater,  $A$  is the surface area of the dummy cell,  $T_a$  is the ambient temperature,  $m$  is the mass of the dummy cell,  $C_p$  is the specific heat capacity of the known material. The step input solution of (5.1) is,

$$\frac{T - T_a}{T_{ss} - T_a} = 1 - e^{-\frac{hA}{mC_p}t} \quad (5.2)$$

where  $T_{ss}$  equals to  $T_a + \frac{\dot{Q}}{hA}$ . In (5.2),  $t$  is the time since the start of heating, and  $T_{ss}$  is the temperature of the dummy cell when it reaches the steady state.

Secondly, when the temperature of the dummy cell reaches the set value, the heater is shutdown and the assembly starts the transient of cooling. During the cooling process,  $\dot{Q}$  equals zero, which means the solution of (5.1) becomes  $e^{-\frac{hA}{mC_p}t}$ . Based on

the above description, once the  $C_p$  is known,  $h$  can be calculated by the following equation,

$$h = -\frac{mC_p}{A} \frac{d[\ln(T - T_a)]}{dt} \quad (5.3)$$

where  $\frac{d[\ln(T - T_a)]}{dt}$  can be obtained by plotting and fitting the curve of temperature  $T$  in MATLAB.

Figure 5.9 shows the fitted curve and the experiment data which are used to calculate the external heat transient coefficient of the Styrofoam assembly. And  $h$  in this case is  $0.69 \text{ W}/(\text{m}^2 \cdot \text{K})$ .

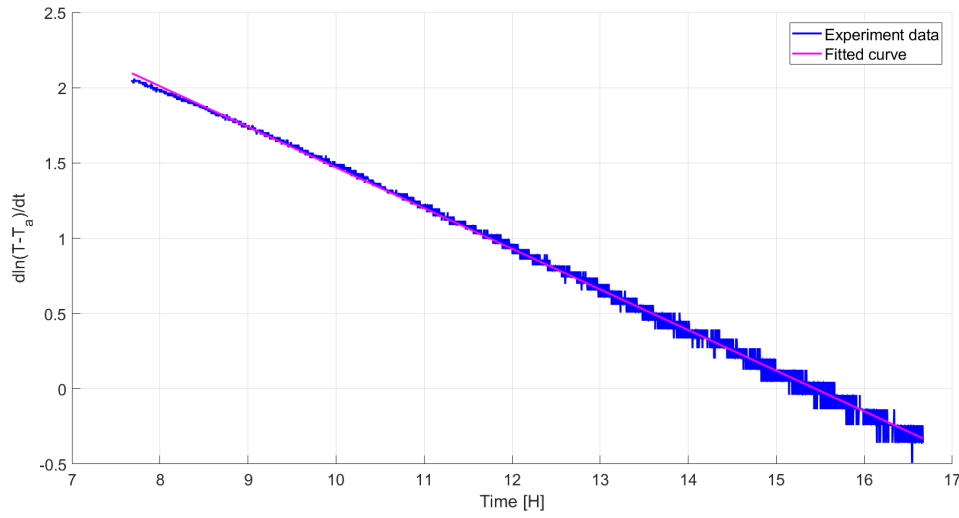


**Figure 5.9:** Fitted curve with experiment data during cooling transient

Finally, the dummy cell is replaced with the actual lithium-ion battery cell, and repeat the same steps as described before. Since the heat transfer coefficient of the assembly is already obtained by (5.3) from the dummy cell test, the specific heat capacity of the battery cell can be calculated by using (5.3) again, which is found to be  $1.19 \text{ J}/(\text{g} \cdot \text{K})$ .





# 6

## Cooling system

### 6.1 Cooling plate design

Different kinds of cooling methods are applied in the automotive industry, and liquid cooling is chosen in this thesis project. A cooling plate is needed to integrate the coolant tube with the test battery. Figure 6.1 shows two different cooling plate designs in Solidworks 3D CAD program. On the left side of the figure, the cooling plate has a design in which the inlet and outlet are close to each other, whereas on the right side, the inlet and outlet are placed far from each other.

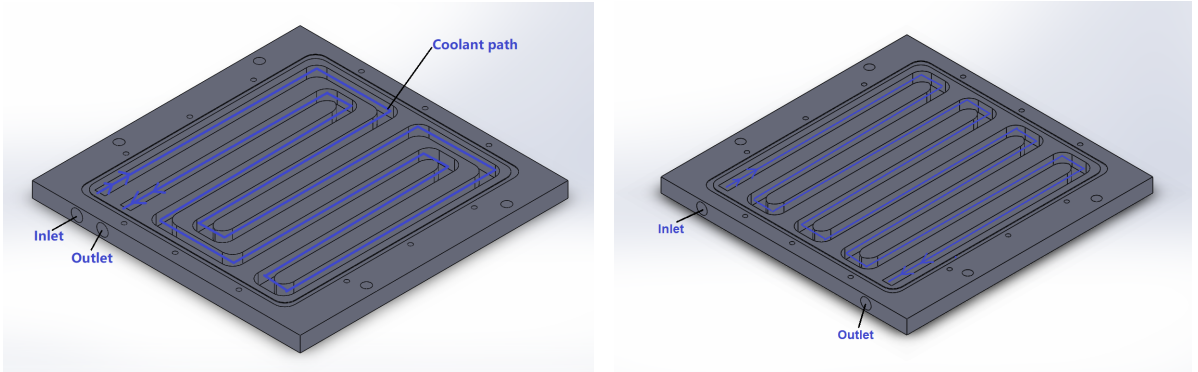


**Figure 6.1:** Design of the cooling plate in Solidworks 3D program

By using the CFD module in COMSOL, the cooling performance of these two designs can be compared. Before the simulation starts, one thing regarding whether the coolant flow is laminar flow or turbulent flow should be decided. Reynolds number ( $Re$ ) can be used to determine the flow status in a pipe, which is governed by the following equation [19],

$$Re = \frac{\rho u D_H}{\mu} = \frac{u D_H}{\nu} = \frac{Q D_H}{\nu A} = 294 \quad (6.1)$$

where  $Q$  is the volume flow rate,  $D_H$  is the hydraulic diameter of the pipe,  $A$  is the pipe's cross-sectional area,  $\nu$  is the kinematic viscosity of the fluid.

The maximum flow rate of this cooling design is 0.1 L/min, and based on the geometry of the cooling pipe, the Reynolds number is 294. This value is less than 2000,

which means it is laminar flow in this project [20]. Then the laminar flow node in COMSOL CFD module can be used to do the simulation and the results are shown in Figure 6.2.

The temperature distribution of the cooling plate is shown in the above figure when the same heating power is applied. It can be seen that when using the first design, the overall temperature of the the plate is lower, and the temperature difference between the inlet and outlet is smaller. This means the left cooling plate design can give a more even temperature distribution on the battery cell temperature.

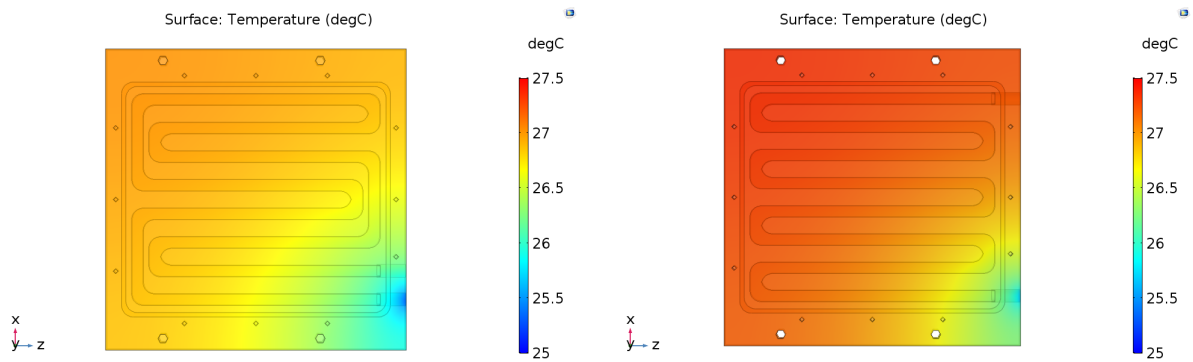


**Figure 6.2:** COMSOL simulation results

Aluminum is used to make the cooling plate, since it has high thermal conductivity and light density. The cooling plate consists of a base and a lid, and the thickness of the base is 12mm, while the thickness of the lid is 3mm, which means the total thickness of the cooling plate is 15mm. The coolant path is carved on the base by using a milling machine. Figure 6.3 gives the physical map of the cooling plate.

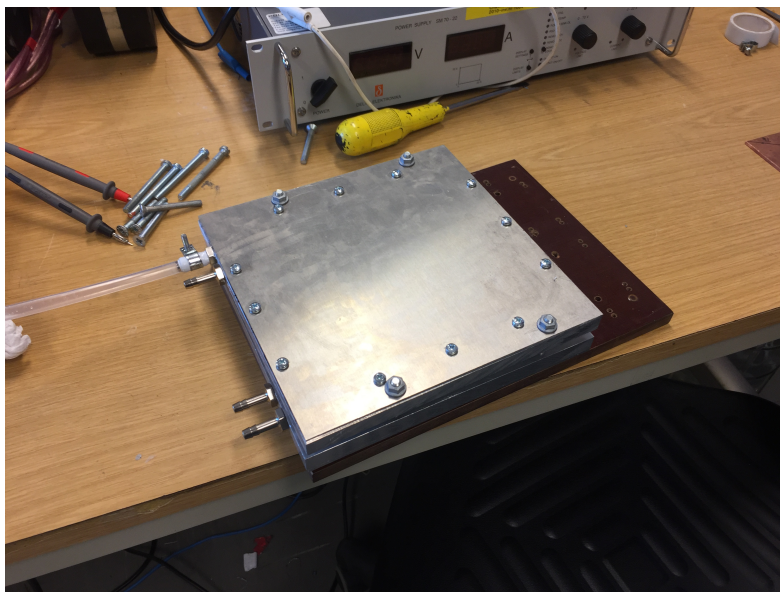


**Figure 6.3:** Physical map of the cooling plate

## 6.2 Physical setup

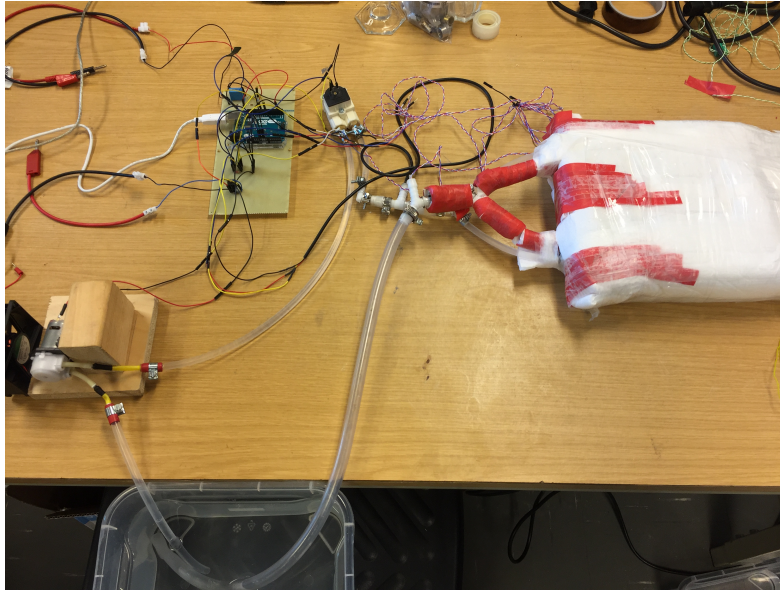


**Figure 6.4:** Physical setup of the cooling system

After the cooling plate is designed and manufactured, the next step is to connect the pump, flow meter and cooling plate with coolant pipes together. The physical setup of the cooling system is shown in Figure 6.4. One thing that should be mentioned is that the battery cell with cooling plate assembly is wrapped with thermal insulation material, which is covered by the red tape in Figure 6.4. As discussed in the thermal chapter, the heat generated by the cell can be trapped by wrapping this thermal insulation material, while the size of the whole assembly is much smaller than the Styrofoam box. The thermal parameters has to be recalculated for the new setup.

## 6.3 Control of the cooling system

By using different libraries in Arduino, the bang-bang control and PID control method can be chosen to control the cooling system. Appendix 1 gives the Arduino code of bang-bang control and PID control. In this project, to demonstrate the concept of controlled cooling system, the bang-bang control method is chosen to perform the experiment.

The pump in the cooling system is driven by a 12V DC motor, and the pulse width modulation can be used to control the average input voltage to the pump. One way to carry out this is to connect one MOSFET in the circuit, and inject the PWM signal to the gate terminal, then by tuning the PWM signal, the average output voltage can be controlled thereby the speed of the cooling pump is controlled. The connection between the pump and Arduino is given in Figure 6.5.

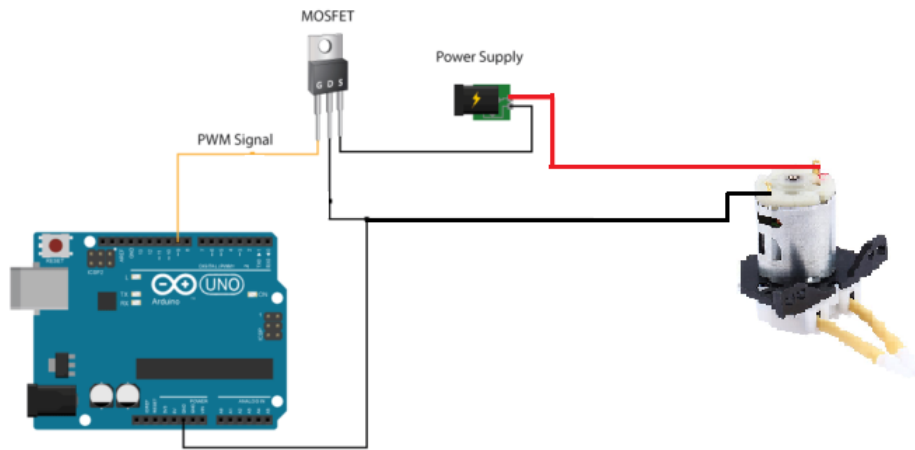


**Figure 6.5:** The schematic of the connection between the pump and Arduino

### 6.4 Performance of cooling system

To evaluate the performance of the cooling system in this project, one pulse test is designed to charge and discharge the battery, and the temperature response of the battery is captured under the situation without and with the cooling. The pulse test sequence is: 15 min of 30 A discharge, 20 min of 1.3 A discharge, 15 min of 30 A charge, 20 min of 1.3 A Charge. The current 30 A and 1.3 A were chosen for simulating a high power and a low power situation.

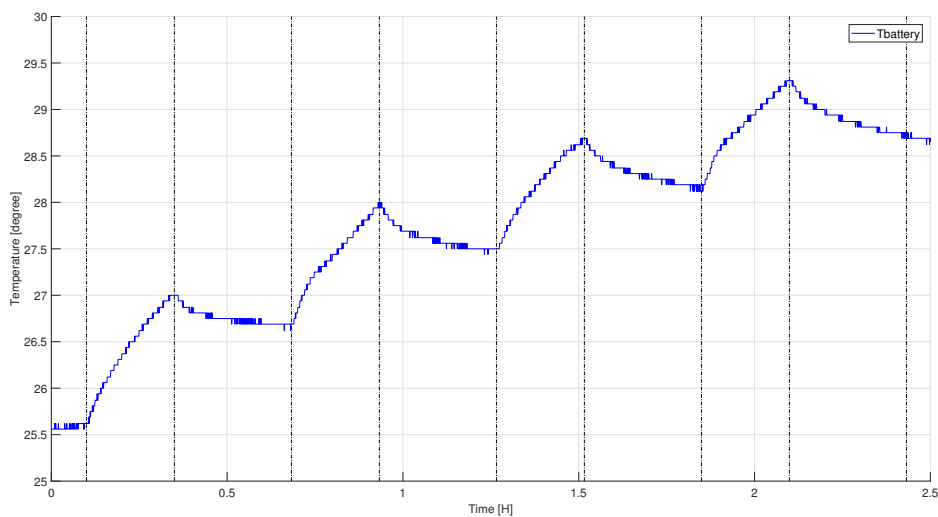


**Figure 6.6:** Battery temperature without cooling

Figure 6.6 gives the battery temperature response in the situation where the cooling system is not applied. It can be seen that the temperature increased up to 29.3°C in the end.

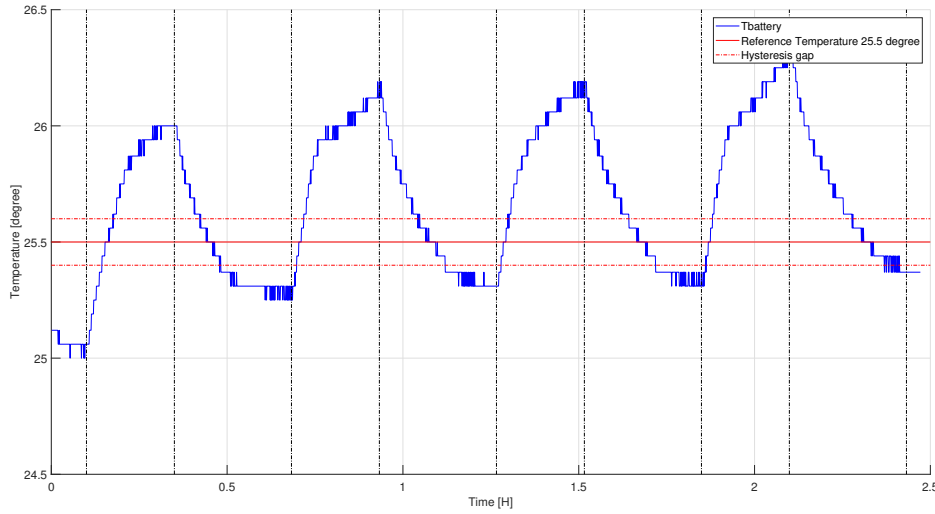


**Figure 6.7:** Battery temperature with cooling

Figure 6.7 shows the battery temperature response with the bang-bang controlled cooling system. The reference temperature for the cooling system is 25.5 °C, and the hysteresis gap for the bang-bang control is from 25.4 °C to 25.6 °C. It means when the temperature is lower than 25.4 °C, the cooling system is OFF; when the temperature is higher than 25.6 °C, the cooling system is ON. It can be seen that the cooling system managed to control the battery temperature, compared to the results in Figure 6.6. However, the battery temperature shows an increasing trend even though the cooling system is engaged. This indicates there is a limitation of this cooling system, which is caused by the low capacity of the pump. If one more powerful power had been used, the performance of the cooling system would have been more in line with expectations.

## 6.5 Simulation of cooling system in MATLAB

In order to verify the performance of the cooling system, a MATLAB Simulink model was built. Since there are several limitations in the practical setup, the model can help to verify more scenarios, such as different power losses and cooling power levels.

### 6.5.1 Thermal model establishment

The model was assumed as a lumped parameter thermal model, which is also a first order RC model, as shown in Figure 2.5. The experiment was done by placing a heater and producing a step input power, in order to see the temperature response, which is shown in Figure 6.8. By using the curve fitting method again, the parameters  $R$  and  $C$  can be identified and they are found to be to 3.64 K/W and 4411.00 J/K, respectively.

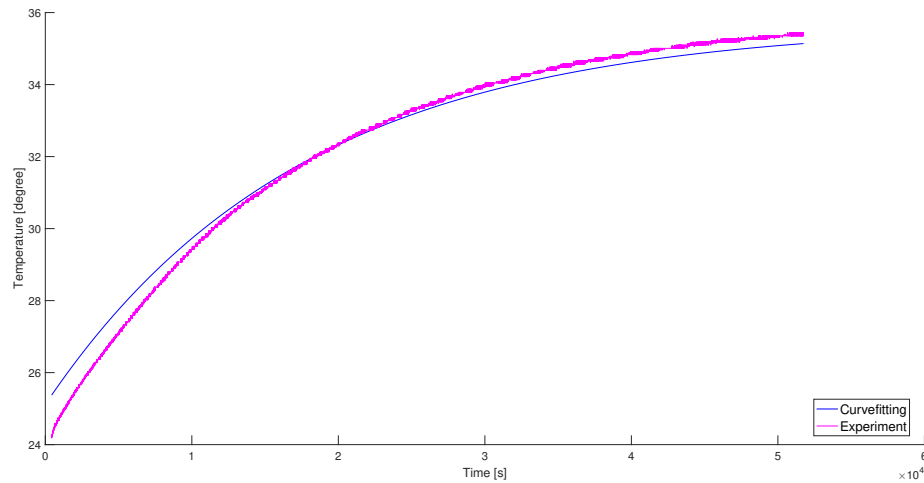


**Figure 6.8:** Simulink model of the system without the cooling

### 6.5.2 Simulink models

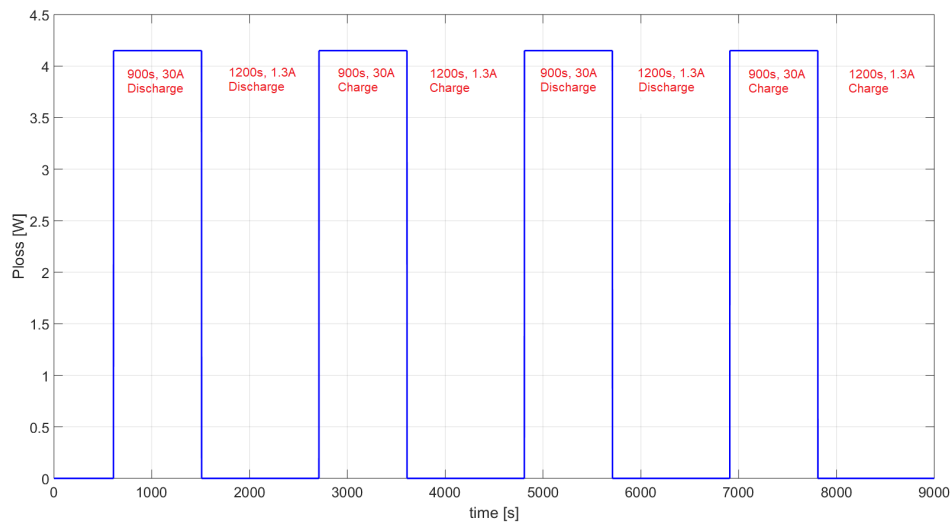


**Figure 6.9:** Charging/discharging power loss profile

With the thermal parameter  $R$  and  $C$ , a Simulink model was built and Figure 6.10 shows the model without the cooling system. The "ploss.mat" represents the heat generated by the battery when charging/discharging, and it is shown in Figure 6.9. The transfer function block in the middle represents the thermal RC model. In addition, the convection power loss was also expressed in this model.

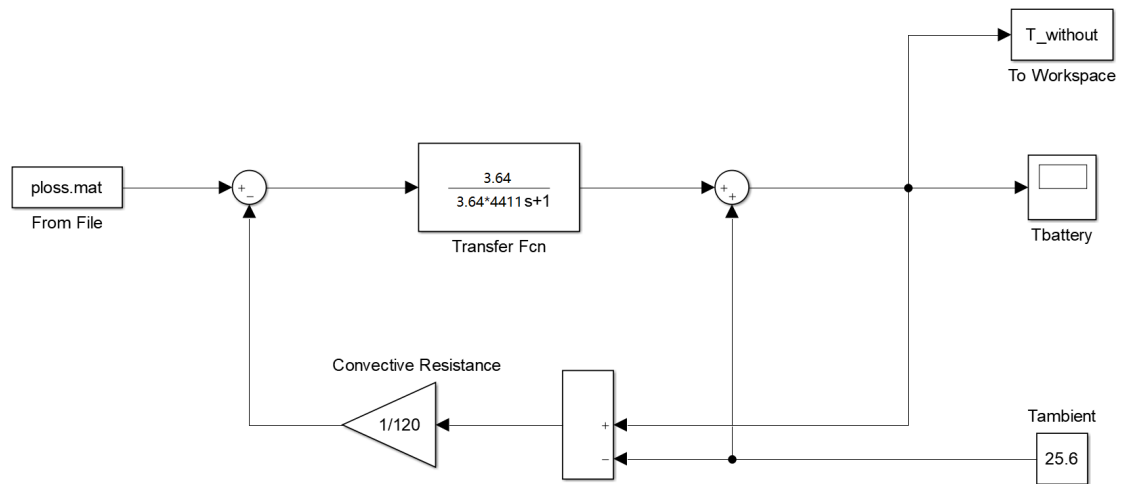


**Figure 6.10:** Simulink model of the system without the cooling

Figure 6.11 shows the model with the cooling system in Simulink. The bang-bang controller generates a 2 W cooling power when the battery temperature is higher than 25.6 °C; it will be OFF when the battery temperature is lower than 25.4 °C.

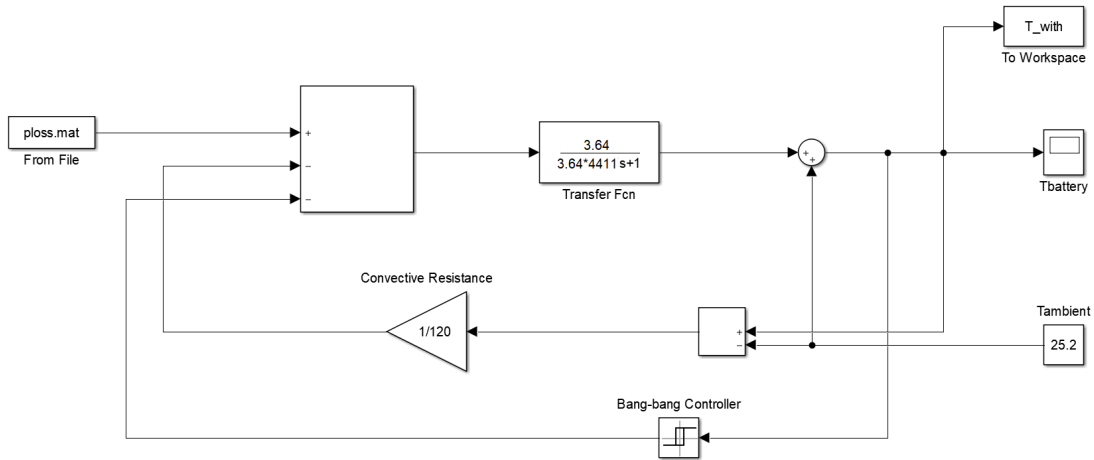


**Figure 6.11:** Simulink model of the system with the cooling

### 6.5.3 Comparison between the practical cooling system and the simulation

In Figure 6.12, the error between the practical and simulation cases can be observed, about 1.4 °C in average. And in Figure 6.13, the designed bang-bang cooling algorithm was added and the error becomes even larger. The error indicates that there is a mismatch of the thermal resistance and capacity. Also, the exponential trend cannot be observed in the simulated curve, which means the lumped parameter thermal model is not detailed enough to represent the practical one.

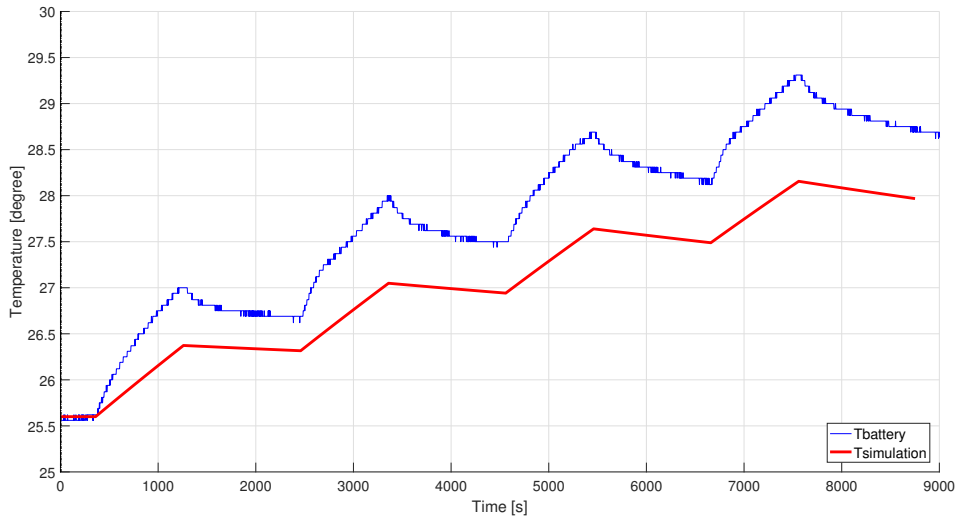


**Figure 6.12:** Comparison between the experiment and the simulation (without cooling)

In Figure 6.13, larger errors can be observed due to the fact that the cooling power was estimated. The flow rate was not stable when the cooling system was running in the beginning. In addition, the temperature difference between the inlet and outlet of the cooling plate is always changing.

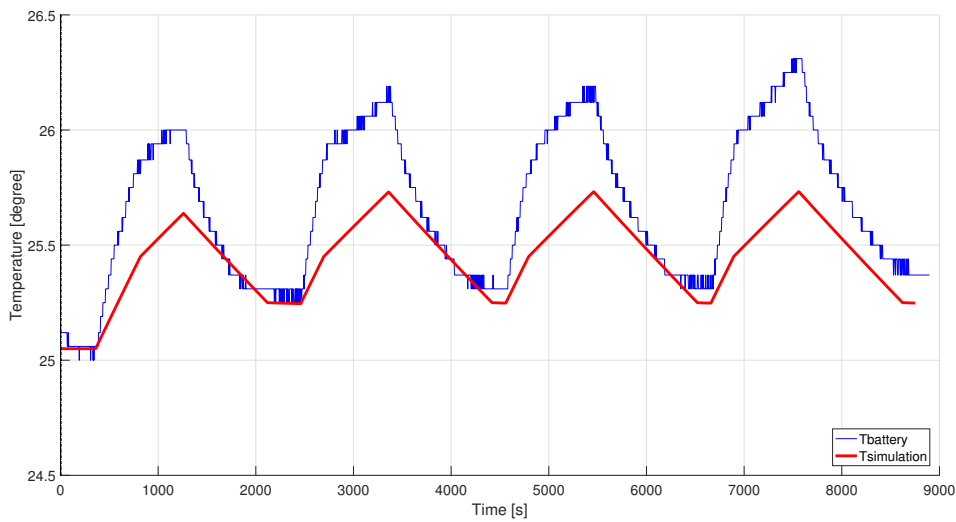


**Figure 6.13:** Comparison between the experiment and the simulation (with cooling)

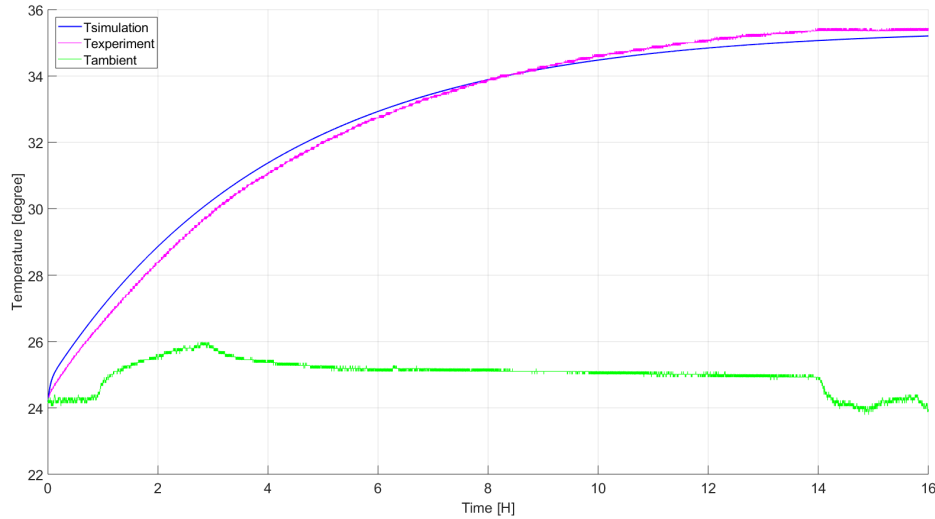
### 6.5.4 Model modification

Two reasons may lead to the errors in the above simulation, one is the inaccurate first order RC thermal model, another is the inaccurate input power losses. These



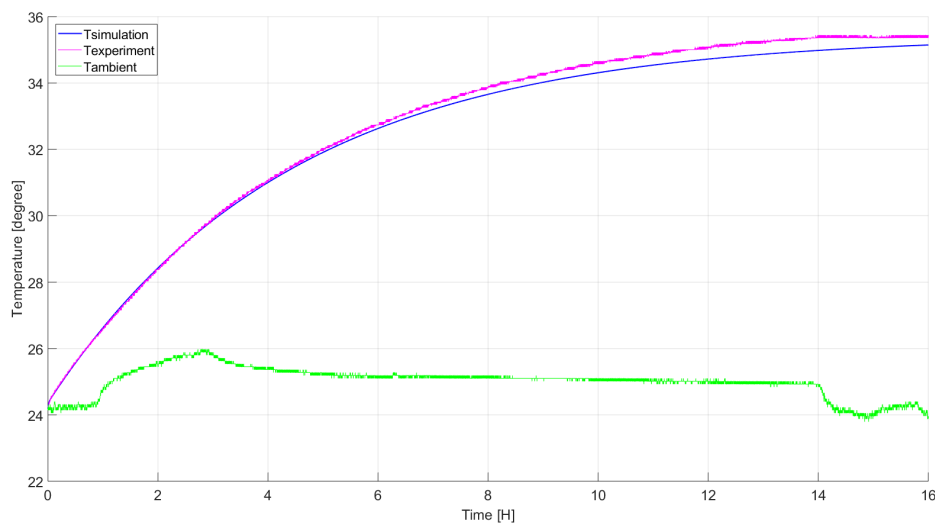


Figure 6.15, when the power step is applied on the model, the error between the simulation and experiment is relatively high in the first few hours. This means the  $R$  parameter of the first branch is too big when using the estimated battery cell thermal conductivity, and it needs to be modified.



**Figure 6.15:** Comparison between the experiment and simulation results when using two RC branches

The least-square curve fitting method is used here again, and the modified parameters are listed in Table 6.1. And the comparison between the experiment and simulation with modified RC parameters is shown in Figure 6.16.



**Figure 6.16:** Comparison between the experiment and simulation results when using modified 2 RC branches parameters

**Table 6.1:** Thermal parameters of 2 RC branches

Thermal parameters	R1	C1	R2	C2
Before modification	0.27 K/W	658.86 J/K	3.37 K/W	3752.14 J/K
After modification	0.08 K/W	658.86 J/K	3.56 K/W	3752.14 J/K

#### 6.5.4.2 Power losses modification

From Figure 6.13, it can be seen that when applying the predefined power on the model, the temperature difference between the simulation and experiment is large, which means the power loss profile is not accurate enough and it needs to be modified as well.

By comparing the temperature difference between the practical and simulated system, the power loss step value is increased from 4.16 W to 5.40 W.

#### 6.5.5 Comparison between the practical cooling system and the simulation after modification

After modification, and when the cooling system is not applied, the experiment and simulation results are shown in Figure 6.17. It can be seen that the simulation result after modification is close to experiment, which means this modified thermal model can be used to represent the actual battery cell.

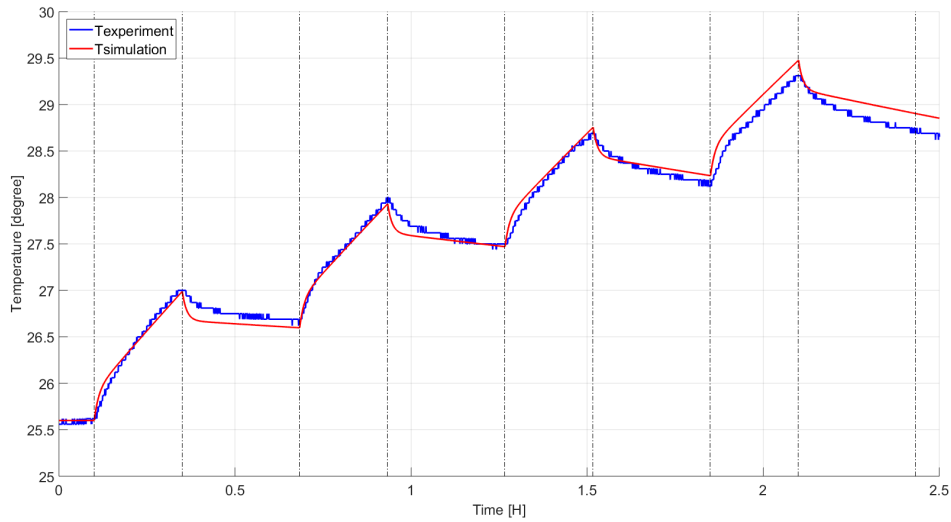


**Figure 6.17:** Comparison results between the experiment and simulation results (after modification, without cooling)

When the same cooling system is applied, the experiment and simulation results are shown in Figure 6.18. It can be seen that the experiment and simulation results have the same trend. The cooling power of the cooling system is around 2W in this case, which can be found that it is hard to regulate the battery temperature in the

required range. However, since a relatively accurate battery cell assembly model has already been got, different simulations regarding different cooling power can be conducted to check the control ability of the cooling system.

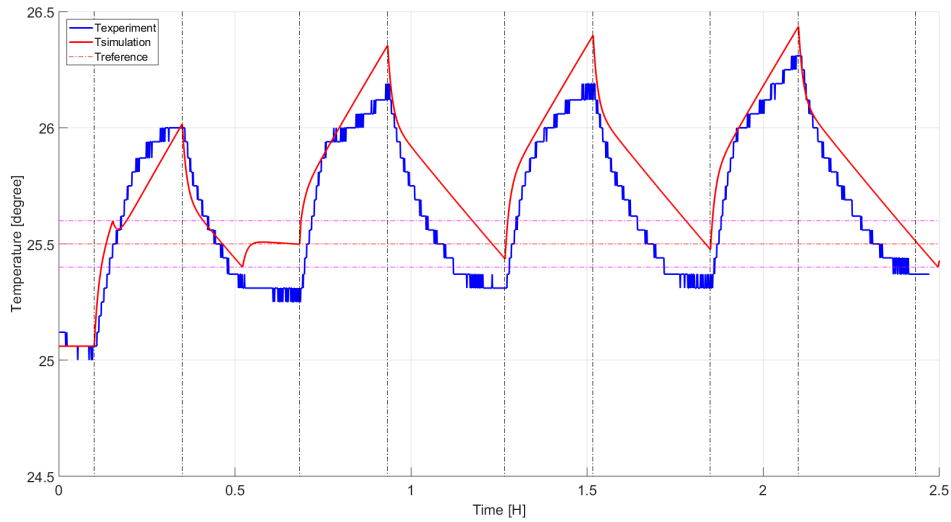


**Figure 6.18:** Comparison results between the experiment and simulation results (after modification, with cooling)

### 6.5.6 Simulation with more powerful pump scenarios

The simulation results of 4 W and 6 W cooling power are shown in Figure 6.19 and Figure 6.20, respectively. And it can be concluded that when the cooling power is more than 6 W, which is treble of the original cooling power, the battery can be controlled within the required temperature range.

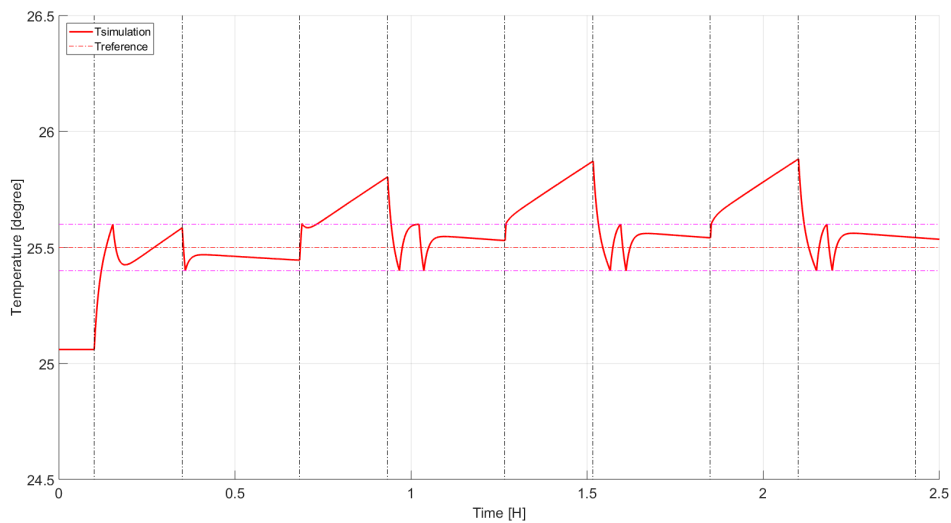


**Figure 6.19:** Simulation results with 4 W cooling power

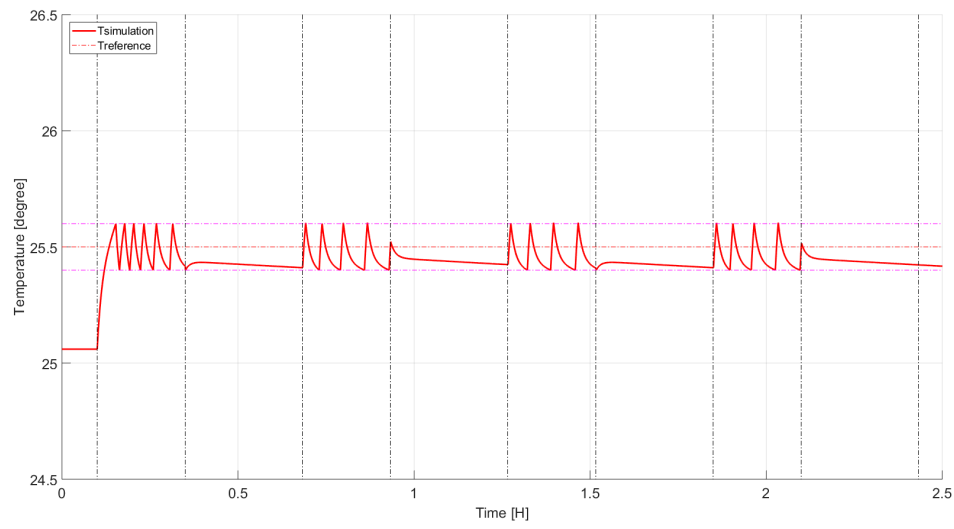


**Figure 6.20:** Simulation results with 6 W cooling power



# 7

## Discussion

### 7.1 Conclusion

By conducting pulse tests, the battery's discharging waveforms have been obtained therefore the RC parameter could be identified, which varies with the SOC levels and ambient temperature. The electrical model was validated by MATLAB Simscape and the simulations and the actual experiments match quite well.

The thermal model establishment started from determining the thermal parameters of the Styrofoam box by using an additional heater. And the thermal resistance is 7.6 K/W and the thermal capacity is 4635.8 J/K. Then a 1C battery discharge test was performed. The electrical and thermal model were coupled together and the error is less than 1 degree. In addition, the specific heat capacity of the battery was also decided, which is 1.19 J/(g·K).

A cooling system with the bang-bang control was designed and tested with the physical set-up. Two designs of the cooling plate in the cooling system was investigated and one was chosen. Water was used in the cooling system as the coolant. A pump, a flow-meter and two temperature sensors were integrated in the system to measure the flow rate and coolant temperature. An Arduino micro-controller was used to control the cooling system. Also, the performance of the cooling system was evaluated and it showed that the designed cooling system managed to control the temperature. Moreover, a more powerful pump can do better job to regulate the battery temperature.

In order to have a more accurate modeling and a better cooling system, the following future work can be done. Firstly, a durable dosing pump shall be used, which should provide a more constant flow of water. An extra cooling fan will also be added, since the pump may be out of function because of the overheat of the motor. Secondly, the electro-thermal model shall be tested with a real driving cycle, such as NEDC, to further validate the model. The battery shall also be validated and tested under different temperatures. Thirdly, the PID feedforward control algorithm shall be implemented in the practical setup. With the charging/discharging current as the input, this algorithm shall be able to estimate the behaviour and action in advance to the overshoot of the temperature. Lastly, more cooling plate designs can be investigated via COMSOL, which may increase the performance of the cooling system.





# Bibliography

- [1] EC, “Regulation (EC) No 443/2009 to define the modalities for reaching the 2020 target to reduce CO<sub>2</sub> emissions from new passenger cars,” *Official Journal of the European Communities*, vol. L 269, no. September 2009, pp. 1–15, 2009.
- [2] F. T. Wagner, B. Lakshmanan, and M. F. Mathias, “Electrochemistry and the future of the automobile,” *Journal of Physical Chemistry Letters*, 2010.
- [3] L. Guzzella, A. Sciarretta *et al.*, *Vehicle propulsion systems*. Springer, 2007, vol. 1.
- [4] L. Ianniciello, P. H. Biwolé, and P. Achard, “Electric vehicles batteries thermal management systems employing phase change materials,” *Journal of Power Sources*, vol. 378, no. October 2017, pp. 383–403, 2018. [Online]. Available: <https://doi.org/10.1016/j.jpowsour.2017.12.071>
- [5] F. Saidani, F. X. Hutter, R. G. Scurtu, W. Braunwarth, and J. N. Burghartz, “Lithium-ion battery models: A comparative study and a model-based power-line communication,” *Advances in Radio Science*, vol. 15, pp. 83–91, 2017.
- [6] Q. Zhang, C. Li, and Y. Wu, “Analysis of Research and Development Trend of the Battery Technology in Electric Vehicle with the Perspective of Patent,” *Energy Procedia*, vol. 105, pp. 4274–4280, 2017. [Online]. Available: <http://dx.doi.org/10.1016/j.egypro.2017.03.918>
- [7] M. Decker, T. Fleischer, J. Schippl, and N. Weinberger, *Zukünftige Themen der Innovations- und Technikanalyse*.
- [8] B. Frieske, M. Kloetzke, and F. Mauser, “Trends in Vehicle Concept and Key Technology Development for Hybrid and Battery Electric Vehicles,” pp. 1–12, 2013.
- [9] E. Wikner, “Lithium ion battery aging: Battery lifetime testing and physics-based modeling for electric vehicle applications,” Ph.D. dissertation, Department of Electrical Engineering, Chalmers University of Technology, 2017.
- [10] R. Rao, S. Vrudhula, and D. N. Rakhmatov, “Battery Modeling for Energy-Aware System Design,” *Computer*, vol. 36, no. 12, 2003.
- [11] F. P. Incropera, D. P. DeWitt, T. L. Bergman, and A. S. Lavine, “heat and mass transfer - Incropera 6e,” p. 997, 2007.
- [12] X. Lin, H. E. Perez, S. Mohan, J. B. Siegel, A. G. Stefanopoulou, Y. Ding, and M. P. Castanier, “A lumped-parameter electro-thermal model for cylindrical batteries,” *Journal of Power Sources*, vol. 257, pp. 12–20, 2014.
- [13] A. Punia, A. Yadav, and A. Rohilla, “Classification of control systems,” vol. 1, no. 12, pp. 797–799, 2015.

- [14] S. K. Lucas and S. T. Simakov, "Computations for Bang – Bang Constrained Optimal Control Using a Mathematical Programming Formulation," vol. 5785, pp. 1–14, 2003.
- [15] D. Honeywell, "Chapter 8 PID Control," 2000.
- [16] A. Rahmoun and H. Biechl, "Modelling of Li-ion batteries using equivalent circuit diagrams," *Electrical review*, vol. 2, no. 7, pp. 152–156, 2012.
- [17] Javier Gazzarri, "Lithium Battery Model, Simscape Language and Simulink Design Optimization - File Exchange - MATLAB Central," 2017. [Online]. Available: <https://se.mathworks.com/matlabcentral/fileexchange/36019-lithium-battery-model-simscape-language-and-simulink-design-optimization>
- [18] H. Maleki, "Thermal Properties of Lithium-Ion Battery and Components," *Journal of The Electrochemical Society*, vol. 146, no. 3, p. 947, 1999. [Online]. Available: <http://jes.ecsdl.org/cgi/doi/10.1149/1.1391704>
- [19] G. Batchelor, "An introduction to fluid mechanics (cambridge mathematical library)," 2000.
- [20] B. Eckhardt, "Introduction. turbulence transition in pipe flow: 125th anniversary of the publication of reynolds' paper," 2009.
- [21] A. Lidbeck and K. R. Syed, "Experimental characterization of li-ion battery cells for thermal management in heavy duty hybrid applications."
- [22] M. Muratori, "Thermal characterization of lithium-ion battery cell," 2010.
- [23] F. Richter, P. J. Vie, S. Kjelstrup, and O. S. Burheim, "Measurements of ageing and thermal conductivity in a secondary nmc-hard carbon li-ion battery and the impact on internal temperature profiles," *Electrochimica Acta*, vol. 250, pp. 228–237, 2017.

# A

## Appendix 1

### A.1 Bang-bang control Arduino code

```
#include <OneWire.h>
#include <DallasTemperature.h>
#include <AutoPID.h>

//Definitions
#define FAN 10
#define ONE_WIRE_BUS 8

//Setup Temperature Sensor
OneWire oneWire(ONE_WIRE_BUS);
DallasTemperature sensors(&oneWire);
double Input, setPoint;

void setup()
{
    // start serial port
    Serial.begin(9600);
    sensors.begin();

    // Temperature setup
    sensors.requestTemperatures();
    Input = sensors.getTempCByIndex(1);
    setPoint = 25.5;

    //Setup Pins
    pinMode(FAN, OUTPUT);
    pinMode(ONE_WIRE_BUS, INPUT);
}

void loop()
{
    sensors.requestTemperatures();
    Input=sensors.getTempCByIndex(1);
    double bangRange = 0.1;
```

```

    if (Input < setPoint - bangRange )
    {
        analogWrite(FAN,0);
    }
    else if (Input > setPoint + bangRange)
    {
        analogWrite(FAN,255);
    }
    Serial.print(" ");
    Serial.print(sensors.getTempCByIndex(0));
    Serial.print(" ");
    Serial.print(sensors.getTempCByIndex(1));
    Serial.print(" ");
    Serial.println(sensors.getTempCByIndex(2));
    delay(2000);
}

```

## A.2 PID control Arduino code

```

#include <OneWire.h>
#include <DallasTemperature.h>
#include <PID_v1.h>

//Definitions
#define FAN 10
#define ONE_WIRE_BUS 8

//Setup Temperature Sensor
OneWire oneWire(ONE_WIRE_BUS);
DallasTemperature sensors(&oneWire);

//Setup PID
double Setpoint , Input , Output;
double aggKp=50, aggKi=20, aggKd=5;
double consKp=20, consKi=10, consKd=10;
PID myPID(&Input , &Output , &Setpoint , consKp , consKi , consKd , REVERSE);

void setup(void)
{
    // start serial port
    Serial.begin(9600);
    sensors.begin();

    // Temperature setup
    sensors.requestTemperatures();
    Input = sensors.getTempCByIndex(1);
}

```

```
Setpoint = 27.5;

//PID Setup
myPID.SetMode(AUTOMATIC);

//Setup Pins
pinMode(FAN, OUTPUT);
pinMode(ONE_WIRE_BUS, INPUT);
}

void loop(void)
{
    //Get temperature and give it to the PID input
    sensors.requestTemperatures();
    Input=sensors.getTempCByIndex(1);

    //Compute PID value
    double gap = abs(Setpoint-Input); //distance away from setpoint
    if(gap < 1)
    {
        //Close to Setpoint, be conservative
        myPID.SetTunings(consKp, consKi, consKd);
    }
    else
    {
        //Far from Setpoint, be aggressive
        myPID.SetTunings(aggKp, aggKi, aggKd);
    }
    myPID.Compute();

    Serial.print(" ");
    Serial.print(sensors.getTempCByIndex(0));
    Serial.print(" ");
    Serial.print(sensors.getTempCByIndex(1));
    Serial.print(" ");
    Serial.print(sensors.getTempCByIndex(2));
    //Serial.print(" ");
    //Serial.print(pulse);
    Serial.print(" ");
    Serial.println(Output);

    delay(2000);

    if (Input == -127)
    {
        analogWrite(FAN,255);
    }
}
```

```
}  
else  
{  
analogWrite (FAN, Output );  
}
```